INL/RPT-23-75988

Alternative Materials Literature Review

December 2023

A Review of Alternative Materials for Xenon Capture in Comparison to AgZ-PAN

Emma MacLaughlin & Rachel Umpleby
Idaho National Laboratory

Jonathan Evarts, Brian Riley, and Praveen Thallapally
Pacific Northwest National Laboratory

Idaho National Laboratory

INL is a U.S. Department of Energy National Laboratory operated by Battelle Energy Alliance, LLC

INL/RPT-23-75988
Revision 1

Alternative Materials Literature Review

A Review of Alternative Materials for Xenon Capture in Comparison to AgZ-PAN

Emma MacLaughlin & Rachel Umpleby
Idaho National Laboratory
Jonathan Evarts, Brian Riley, and Praveen Thallapally
Pacific Northwest National Laboratory

December 2023

Idaho National Laboratory
Aqueous Separations and Radiochemistry
Idaho Falls, Idaho 83415

http://www.inl.gov

Prepared for the
U.S. Department of Energy
Office of Nuclear Energy
Under DOE Idaho Operations Office
Contract DE-AC07-05ID14517

Page intentionally left blank

ABSTRACT

A collaborative literature review between Idaho National Laboratory (INL) and Pacific National Laboratory (PNNL) was conducted to research alternative metals/materials for xenon adsorption in gaseous effluents generated from used nuclear fuel (UNF) reprocessing. The review was conducted to research sorbents that could outperform silver mordenite (AgZ) at ambient temperature. The use of silver requires complex and expensive waste disposal processes due to it being an RCRA metal, therefore alternative materials need to be researched and evaluated.

The report details two different types of sorbent material: alternative zeolite materials and non-zeolite-based materials (i.e., MOFs, COFs, etc.). This report documents a brief history of the materials, what testing has been conducted on them, and what results suggest the possibility of outperforming the silver-based materials. Sorbent performance characteristics such as durability, capacity, and operating temperatures were evaluated. The simplicity of the sorbents was also evaluated, meaning how they are acquired (synthesized vs. naturally abundant). Recommendations were made for the most promising sorbents based on available research in the subject area and these recommended sorbents will be tested in the upcoming fiscal year. The recommended sorbents that are zeolite based are CHA zeolites, ZIF-69, and Na-ETS-10. The recommended sorbents that are non-zeolite based are SBMOF-1 and CC3.

ACKNOWLEDGEMENTS

The team would like to thank Amy Welty, Mitch Greenhalgh and Meghan Fujimoto for their leadership and direction throughout the literature review.

Page intentionally left blank

CONTENTS

FIGURES

TABLES

ACRONYMS

AgZ	Silver Mordenite Sorbent
BET	Brunauer-Emmett-Teller
COF	covalent organic framework
CNT	carbon nanotube
GCMC	grand canonical Monte Carlo
HOF	hydrogen-bonded organic framework
IAST	ideal adsorbed solution theory
INL	Idaho National Laboratory
K	kelvin
Kr	krypton
MOF	metal-organic frameworks
MS5A	molecular sieve 5A
OMS	open metal site
PNNL	Pacific Northwest National Laboratory
POC	porous organic cage
Qst	isosteric heat of adsorption
RCRA	Resource Conservation and Recovery Act
UNF	used nuclear fuel
Xe	xenon
ZIF	zeolitic imidazolate framework

Page intentionally left blank

Alternative Metals Literature Review

1. Introduction

A collaborative literature review between Pacific Northwest National Laboratory (PNNL) and Idaho National Laboratory (INL) was conducted to research alternative metals/materials for xenon adsorption in gaseous effluents generated from used nuclear fuel (UNF) reprocessing. Currently, silver mordenite (AgZ) is the most promising sorbent for xenon (Xe) adsorption at room temperature [1]. However, silver is an RCRA metal, which requires more complex and expensive waste disposal. This literature review was conducted to research alternative metals/materials that could outperform AgZ while avoiding RCRA metal usage in the sorbent material. The report details two different types of sorbent material: alternative zeolite materials and non-zeolite-based materials (i.e., MOFs, COFs, etc.). This report documents a brief history of the materials, what testing has been conducted on them, and what results suggest the possibility of outperforming the silver-based materials. Sorbent performance characteristics such as durability, capacity, and operating temperatures were evaluated. The simplicity of the sorbents was also evaluated, meaning how they are acquired (synthesized vs. naturally abundant). Recommendations were made for the most promising sorbents based on available research in the subject area and these recommended sorbents will be tested in the upcoming fiscal year. The recommended sorbents that are zeolite based are CHA zeolites, ZIF-69, and Na-ETS-10. The recommended sorbents that are non-zeolite based are SBMOF-1 and CC3.

1.1 AgZ Sorbent Comparison

INL has patented and tested silver mordenite engineered sorbents for xenon (Xe) capture for over a decade [1]. The characteristics of AgZ that were compared to each sorbent were based off of testing conducted at INL and can be seen in Table 1. For experimental testing and parameter evaluation of AgZ, BET analysis for total surface area was conducted in addition to deep-bed column testing. The deep-bed column testing was performed at ambient temperature (295 K) using a test gas mixture of 1000 ppm xenon (Xe) and 150 ppm krypton (Kr) in a balance of air. Xe capacity and Xe selectivity over other gas constituents were calculated from the adsorption testing results [1].

Table 1. AgZ sorbent characteristics to be compared against sorbents found through the literature review.

Form (engineered form, powder, etc.)	How is it made?	BET Surface Area (m^2/g)	Average Pore Size (Å)	Pore Volume (cm^3/g)	Xe Capacity (mmol/kg)	Xe/Kr Selectivity	Xe/N_2 Selectivity
Engineered Form	Commercially Bought	223	26.797	0.149	51.58	10.9	11.3

2. Alternative Zeolites

Zeolites are a group of hydrated aluminosilicates of alkali or alkaline earth metals; this includes metals such as sodium and potassium. Historically, zeolites have been used as adsorbents for gas and liquid separation or purification in a variety of applications [2]. Zeolites are classified as molecular sieves, similar to activated carbon, which is also used to adsorb constituents from off-gas streams. Due to their vast range of applications, many zeolites are commercially available; however, they may also be synthesized for specific applications [2]. AgZ is a mordenite-based adsorbent, which is a type of zeolite. Alternative zeolite types and alternative metal additions were reviewed; promising options are included in this report.

2.1 X- and Y-Zeolites

X- and Y-Zeolites are faujasite-type zeolites and are considered synthetic. They consist of a cubo-octahedral structure and have SiO^{4-} and AlO^{4-} tetrahedrals at each corner of the framework [2]. The difference between the two is defined by the Si/Al atomic ratio where zeolite X has a Si/Al ratio close to one and zeolite Y has a Si/Al ratio higher than two. The general formulas for both zeolite X and Y respectively are $(Ca, Mg, Na_2)_{29}(H_2O)_{240}[Al_{58}Si_{134}O_{384}]$ and $(Na_2, Ca, Mg)_{3.5}[Al_7Si_{17}O_{48}] * 32(H_2O)$[3]. The X zeolite-metal sorbents reviewed included NaX and LiX. The Y zeolite-metal sorbents reviewed are NaY, Pt/NaY, Ru/NaY, Zn(55)Y, and Zn(74)Y.

Zeolite X was studied with two possible metals: sodium and lithium [4]. Aristov et al., conducted a study that looked at the dependence of both krypton and xenon adsorption with changes in pressure and temperature. Adsorption isotherms were measured in a temperature range of 183-243 K and can be seen in Figure 1. The adsorption of xenon on both sorbents performed better with decreasing temperature. No room temperature testing was conducted. Xenon capacity for each sorbent was also calculated and showed there was very little difference between LiX and NaX sorbents. The average xenon capacity for LiX and NaX was 6.1 and 5.3 mmol/g, respectively [5].

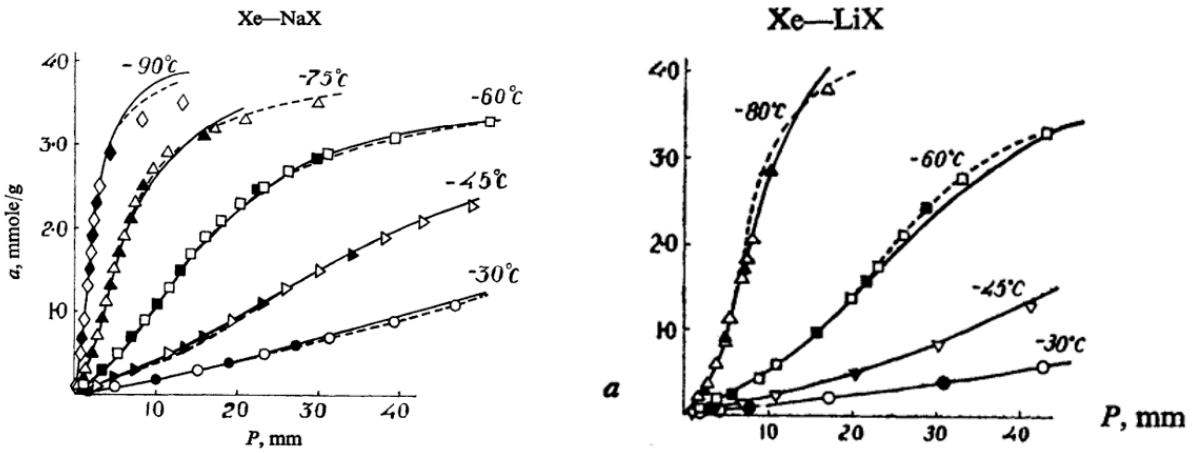

Figure 1. Isotherms of xenon in zeolite NaX (left) and LiX (right) at different temperatures. Solid and dashed lines were calculated from equations while dots are experimental data [5].

Zeolite Y was studied with several metal additions including sodium, platinum, ruthenium, and zinc [6, 7]. A study conducted by Ryoo et al., looked at NaY and the addition of various metals on xenon adsorption. Adsorption isotherms were obtained using pure xenon gas at two temperatures, 296 K and 310 K. The adsorption isotherms can be seen in Figure 2. As seen in the figure, the addition of metals onto zeolite NaY had no real impact on xenon adsorption and the adsorption isotherms were linear for all three zeolite samples [6].

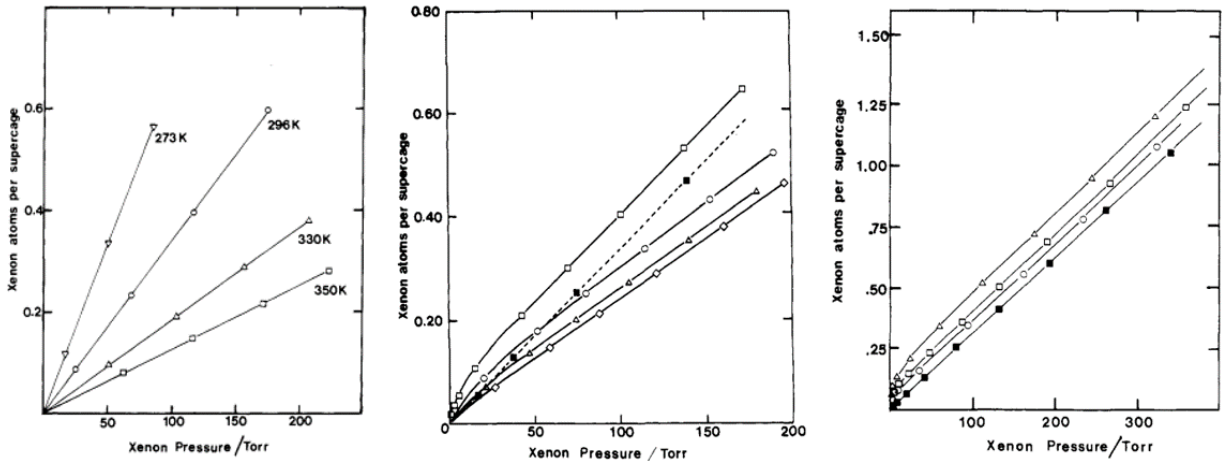

Figure 2. Xenon isotherm adsorption on sorbent NaY at different temperatures (left). Xenon adsorption plotted against pressure: $Pt_{7.1}$/NaY (O), $Pt_{3.6}$/NaY (Δ), and $Pt_{1.4}$/NaY (◊) at 310 K; $Pt7_{7.1}$/NaY (□) and $Pt_{7.1}$/NaY with chemisorbed hydrogen (■) (center). Xenon adsorption plotted against pressure at 296 K: (Δ) $Ru_{9.3}$/NaY; (□) $Ru_{6.2}$/NaY; (O) $Ru_{3.1}$/NaY; (■) $Ru_{9.3}$/NaY with chemisorbed hydrogen [7].

In a separate study by Boddenberg, NaY was tested with varied compositions of zinc added as a metal cluster [7]. This included a 55% and 74% zinc addition. Adsorption isotherms using pure xenon were created using a temperature range of 296 to 309 K, as seen in Figure 3. The addition of zinc onto zeolite NaY had a higher amount of xenon adsorbed compared to the study conducted by Ryoo et al. described above. The adsorption isotherms were still linear and the difference in zinc percentage didn't impact the adsorption [7].

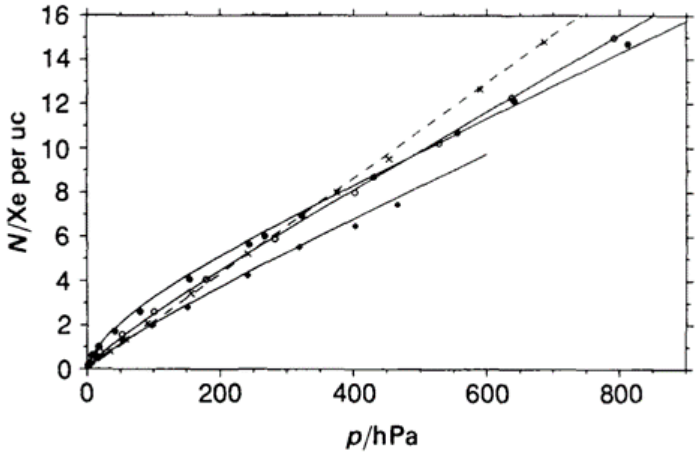

Figure 3. Isotherms for adsorption at 298 K on Zn(55)Y(○) and Zn(74)Y(●) [7].

From the literature review conducted on NaX and NaY derived sorbents, it is evident that they will not outperform AgZ in xenon adsorption. This is mainly due to the poor adsorption isotherms seen at cold temperatures. AgZ has a high capacity for xenon at room temperature, but the NaY derived sorbents had poor xenon adsorption at near room temperature and NaX sorbents were not even tested in this range. The additional requirement for operating at cold temperatures is therefore not justified by increased performance. A direct comparison of sorbent characteristics and test values discussed in this section can be seen in Table B1 of Appendix B.

2.2 Chabazite

Chabazite (CHA) is a tectosilicate mineral in the zeolite group and is naturally occurring. The general formula of $(Ca, K, Na_2)_2[Al_2Si_4O_{12}]_2 * 12H_2O$ [2]. The zeolites reviewed included Na-CHA, Cu-CHA, Pd-CHA, K-CHA, Ca-CHA, Cs-CHA, Rb-CHA, Li-CHA [8, 9, 10].

Torcivia et al. looked at the affinities that Ag, Cu, and Pd functionalized chabazites have for noble gases (Xe, Kr, Ar). Since the goal is to not use RCRA metals, the testing conducted with Ag was not included in this report. Inverse gas chromatography was used to generate adsorption isotherms from a pure gas feed at a range of temperatures (373-473 K), as seen in Figure 4. The adsorption isotherms for all sorbents were very similar showing a logarithmic convergence as xenon partial pressure increased. Ag-CHA had the largest xenon capacity until 0.4 xenon partial pressure, but the results for all sorbents were comparable. Selectivity was calculated for Xe and Kr for each sorbent as well, as seen in Figure 5. All sorbents were selective for xenon over krypton. Ag-CHA had the highest selectivity for Xe out of all the tested sorbents, but Na-CHA, Pd-CHA, and Cu-CHA all had similar selectivity values to each other for the entire temperature range. All sorbents had an overall higher selectivity at lower temperatures, but reported data stopped a 373 K, so more testing is required to determine the selectivity at room temperature to do a full comparison to AgZ [8].

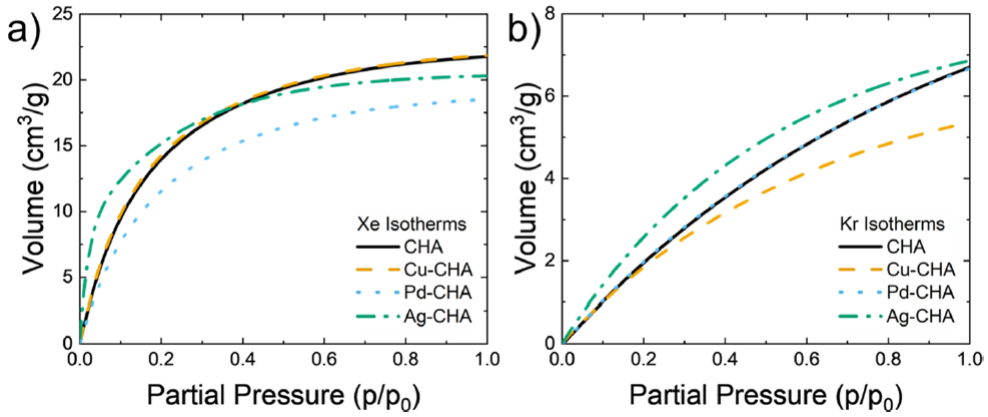

Figure 4. Isotherms for Xe (a) and Kr (b) adsorption at different temperatures. [8]

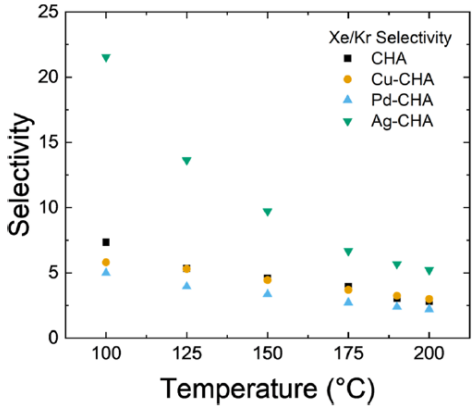

Figure 5. Selectivity for Xe over Kr of CHA-derived sorbents at different temperatures. [8]

Another study conducted by Torkia et al. looked at adsorption isotherms for xenon on Ca-CHA, Cs-CHA, Li-CHA, K-CHA, and Rb-CHA [10]. All testing was conducted at room temperature using pure xenon gas and adsorption isotherms were obtained at varying pressures, as seen in Figure 6. For these

sorbents, the adsorption isotherms were more linear than compared to the other CHA sorbent report previously discussed. In addition, xenon capacity was calculated for Ca-CHA, Cs-CHA, Rb-CHA, K-CHA, and Li-CHA and is shown in Table 2. From the figure and xenon capacity values in the table, Ca-CHA performed the best [10].

Table 2. Xenon Capacity for CHA-based sorbents [10].

Sorbent	Xenon Capacity (mmol/g)
Ca-CHA	2.36
Cs-CHA	0.18
Rb-CHA	1.08
K-CHA	1.89
Li-CHA	1.9

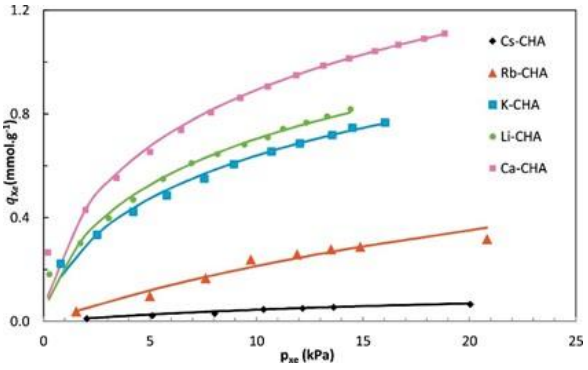

Figure 6. Xe adsorption isotherms for CHA-derived sorbents at 298 K. [10]

Several CHA-derived sorbents could be promising in outperforming AgZ for xenon adsorption. This conclusion is based on the selectivity of the sorbents seen at different temperatures. Pd-CHA, Ca-CHA, and Cu-CHA had high selectivity for Xe over Kr at lower temperatures. The adsorption isotherms for those sorbents were also comparable to the testing of Ag-CHA. Additional testing conducted at ambient temperature would aid in understanding if these sorbents are promising at xenon adsorption. The study conducted by Torkia et al. compared other CHA-derived sorbents, the xenon capacity values, and adsorption isotherms were comparable to outperformed AgZ at room temperature. Further testing to see how the sorbents' selectivity of xenon would need to be conducted.

2.3 Mordenite

Mordenite is an abundant type of zeolite that is found naturally in volcanic deposits [2]. Kuznicki performed a study on Na-ETS-10 and its counterpart, Ag-ETS-10 [11]. For the testing, Na-ETS-10 beads were packed into columns and injected with test gas at a temperature range of 298-373 K. Adsorption isotherms at 298 K were calculated for both adsorbents and can be seen in Figure 7. Ag-ETS-10 had a higher xenon adsorption compared to Na-ETA-10, but due to its RCRA metal composition, Ag-ETS-10 is not being further investigated. Na-ETS-10 did have a better adsorption curve compared to previously reported sorbents in this report. In addition, the selectivity for Xe/N_2 was calculated for Na-ETS-10 and was found to be 13-18 for the temperature range tested [11]. This is higher than the Xe/N_2 selectivity AgZ has and more testing should be done to evaluate the sorbent as a possible alternative to AgZ.

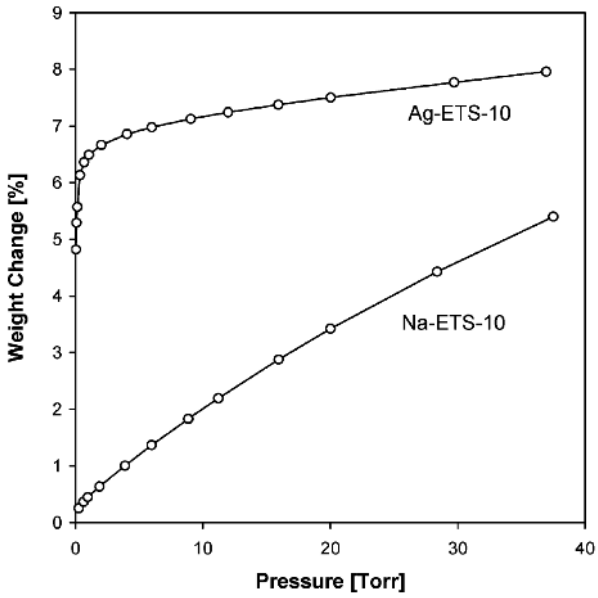

Figure 7. Xe adsorption isotherm obtained using Na-ETS-10 and Ag-ETS-10 at 273 K. [11]

2.4 Abstract Zeolite Sorbents

2.4.1 Molecular Sieves

Molecular sieves are synthetic crystalline zeolites that have their atoms arranged in a definite pattern [2]. The reviewed molecular sieves included molecular sieve 5A (MS5A), Koestrolith 13X-K2, and Koestrolith 4K [12, 13]. A study was conducted by Munakata et al. on the adsorption equilibria of Kr, Xe, and N_2 on molecular sieve 5A [12]. It focused on obtaining adsorption isotherms for the sorbent using pure gas components (K, Xe, and N2) and a binary component gas stream (Kr and Xe). The testing was conducted at a range of temperatures. The temperature range for pure gas component testing was 77 K to 353 K and the temperatures used for binary gas component testing were 195 K and 273 K. The adsorption isotherms for both Kr and Xe at specific temperatures can be seen in Figure 8. As can be seen in the figure, MS5A adsorbs the same amount of Kr and Xe at each pressure value tested and never exceeds 0.01 mol/g for either species. This shows that it is poor at absorbing either species, and it does not have selectivity for either species. It is a poor sorbent compared to AgZ in xenon adsorption [12].

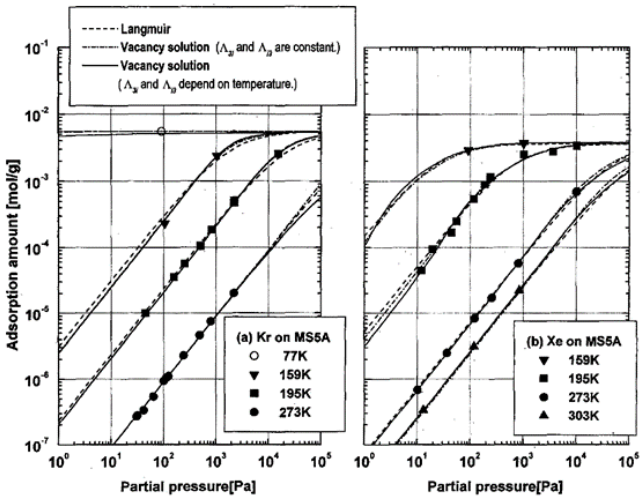

Figure 8. Adsorption isotherms for Kr (left) and Xe (right) on MS5A at different temperatures. [12]

Koestrolith 13X-K2 and Koestrolith 4AK are also commercial molecular sieves with a different structure than MS5A [13]. Adsorption isotherms were obtained for both sorbents at 303 K using pure gas components (Ar, Kr, Xe, and O_2). These can be seen in Figure 9. Adsorption equilibria data was also obtained at 303 K using a mixed gas stream (Kr/Ar, Xe/Ar, Xe/Kr, O_2/Ar, Kr/O_2, Xe/O_2). As seen in the figures, both sorbents selectively adsorbed xenon, yet Koestrolith 13X-K2 had a higher capacity for xenon than Koestrolith 4AK. Koestrolith 13X-K2 outperforms Koestrolith 4AK with Xe capacity values an order of magnitude higher. Koestrolith 13X-K2 had a xenon capacity of 11.344 mmol/g, whereas Koestrolith 4AK had a xenon capacity of 3.918 mmol/g [13].

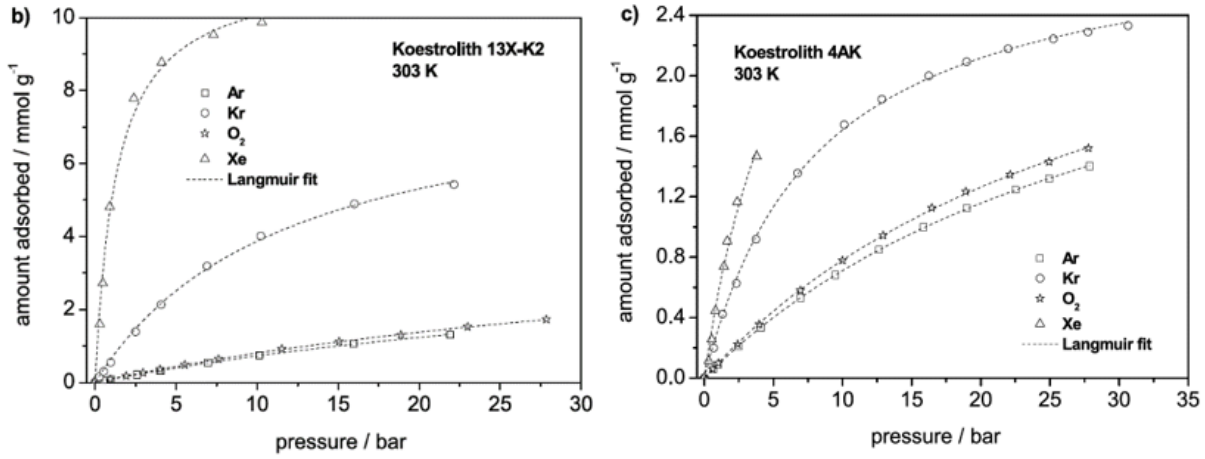

Figure 9. Adsorption isotherms of Ar, Kr, O2, and Xe when using Koestrolith 13X-K2 and Koestrolith 4K at 303 K. [13]

2.4.2 Zeolitic-Imidazolate Frameworks (ZIFs)

ZIFs are zeolitic-imidazolate framework sorbents, and the sorbent reviewed was ZIF-69 [14]. ZIF-69 was tested in a study conducted by Shihui in 2020, making this sorbent a relatively new synthetic zeolite [14]. Single component testing was performed with pure Xe and Kr gas adsorption isotherms at temperatures ranging from 273–298 K. Xe capacity was calculated at 2.46-3.56 mmol/g with respect to the temperatures stated previously. In addition, ZIF-69 has a Xe/Kr selectivity of 8.35, which is lower than the AgZ Xe/Kr selectivity calculated at 295 K, being 10.9 [14].

2.4.3 RHO Zeolites

RHO zeolites are synthesized zeolites. RHO zeolites were synthesized for a study conducted by Tsiao et al., to obtain adsorption isotherms at a range of temperatures for pure xenon at various pressures [15]. Pure gas component tests were conducted at temperatures ranging from 195 – 300 K. Cesium (Cs) concentrations were varied for the composition of the RHO zeolites to see the impact it would have on xenon adsorption. The Cs concentrations tested were 0.75 cesium per unit cell (Cs/uc) and 2.0 Cs/uc. Adsorption isotherms for both Cs concentration sorbents at 300 K are seen in Figure 10. Included in the figure below is a focus on the 0.75 Cs/uc concentrated sorbent at various temperatures. Due to the 0.75 Cs/uc sorbent outperforming the other sorbents tested, more focus was put on this sorbent. From the figure, it is seen that this sorbent adsorbs more xenon at lower temperatures compared to room temperature [15].

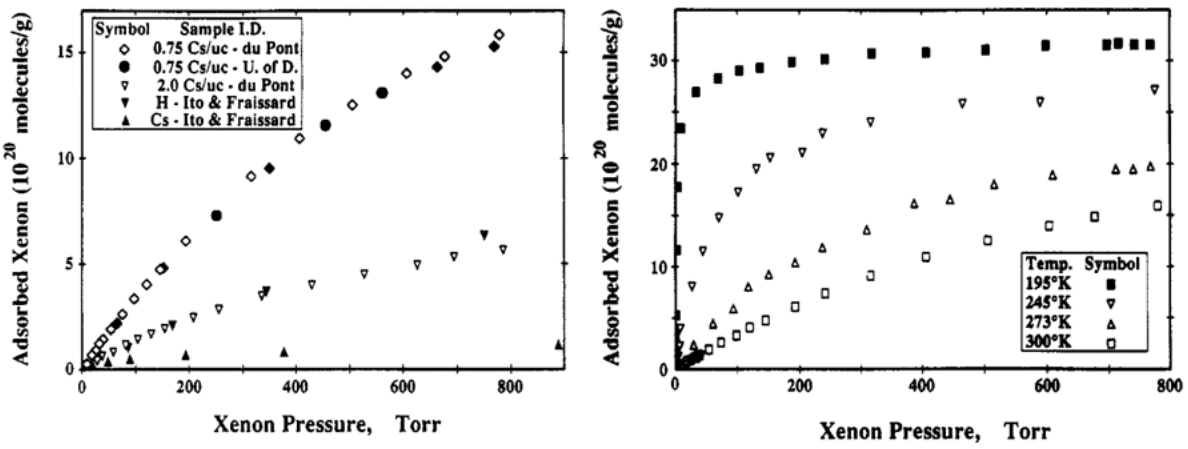

Figure 10. (Left) Xe adsorption isotherms obtained using RHO zeolites with varying Cs concentrations at 300 K. (Right) RHO zeolite (0.75 Cs/uc) isotherm at different temperatures. [15]

3. Alternative Materials

Alternative materials, specifically organic materials, were reviewed in order to evaluate a sorbent that will outperform AgZ for Xe capture. The organic materials reviewed included metal organic frameworks (MOFs), covalent organic frameworks (COFs), porous organic frameworks (POCs), hydrogen-bonded organic frameworks (HOFs), and nanoporous solid sorbents.

3.1 Metal Organic Frameworks

One of the first investigations to use MOFs to separate Xe and Kr was Mueller et al. where MOF-5 was the most promising candidate [22]. Following this demonstration, many other investigations began to study the use of MOFs to separate noble gases. For example, Thallapally et al. [20] investigated MOFs with open-metal-sites (OMSs) to separate Xe from Kr at ambient temperature (see Figure 11). Results were compared to activated carbon, which is a typical material used in Xe capture. In pure component gases, NiDOBDC MOF is more selective for Xe over Kr with an uptake ratio of 5-6 compared to 3.8 for charcoal [20]. Under simulated nuclear reprocessing off-gas (400 ppm Xe, 40 ppm Kr balanced with air), the NiDOBDC MOF adsorbed 4.8 mmol/kg of Xe and 0.066 mmol/kg of Kr at room temperature.

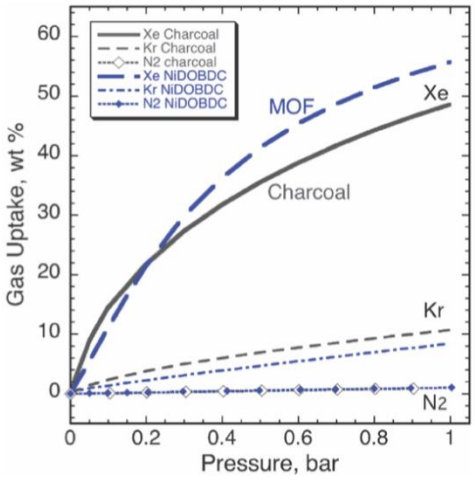

Figure 11. Xe, Kr, and N2 adsorption isotherms at room temperature for NiDOBDC and activated carbon. [20]

Separation of Xe and Kr can be achieved through their differences in kinetic diameters (Xe: 4.047 Å, Kr: 3.655 Å) and polarizabilities (Xe: 40.44×10^{-25} and Kr: 24.84×10^{-25} cm^3) using a molecular sieve-type approach, as discussed in the previous section. Separation by kinetic diameter differences is accomplished through careful design of material pore size, where optimal pore size is approximately 4–8 Å [23, 24]. In terms of polarizability, metal cations can enhance the interaction with polarizing adsorbents as shown in the NiDOBDC MOF [20]. Although there is not a one-size-fits-all formula to determine Xe/Kr selectivity, there are some general features that improve selectivity, such as low void fractions, very high Xe energies, and pore sizes approximately equivalent to that of the Xe atom [18]. Perhaps counterintuitively, materials with lower surface area tend to exhibit higher selectivities [18].

In a study by Simon et al. [18], a literature review covering 670,000 different materials from the *Nanoporous Materials Genome* was used to evaluate potential candidates for separation of Xe and Kr at ambient temperature. This study utilized a combination of random forest machine learning algorithms and molecular simulations, which were back correlated to three pore models to determine the strongest candidates with links between selectivity and pore size and included a range of nanoporous materials including MOFs, COFs, and zeolites (see Figure 12). The two strongest candidates found for Xe/Kr selectivity were an aluminophosphate zeolite (JAVTAC), produced by Cooper et al, [25] and a calcium-based material [SBMOF-1(KAXQIL)], produced by Banerjee et al. [26].

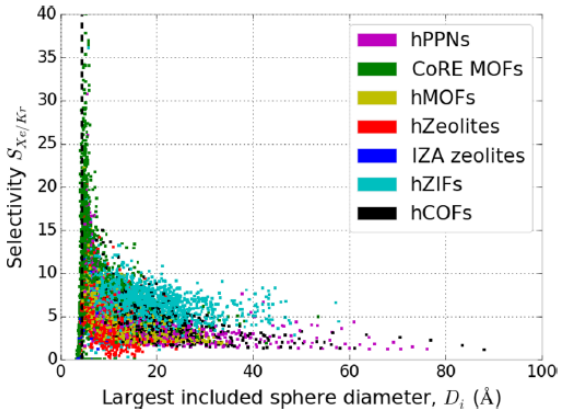

Figure 12. Xe/Kr selectivity versus diameter of the largest included sphere. Simon et al. [18]

Figure 13 provides a comparison of state-of-the-art Xe/Kr separation materials as a function of the Henry coefficient. Values reported from the literature show that SBMOF-1 displayed the highest Henry coefficient and Xe/Kr selectivity, indicating excellent performance under used nuclear fuel (UNF) reprocessing conditions and in agreement with previous studies. Further testing found that SBMOF-1 removes 13.2 mmol Xe kg^{-1} of a simulated UNF reprocessing off-gas [19]. In addition to its high selectivity, SBMOF-1 adsorption performance is preserved during thermal cycling and is stable up to 500 K. Single-crystal X-ray diffraction revealed in Xe-loaded SBMOF-1, the Xe adsorbs near the midpoint of the channel through Van der Waals interactions [19]. In a similar study, Banerjee et al. used molecular simulations to screen 125,000 MOF structures to identify highly selective MOFs for Xe gas capture in conditions representative of UNF reprocessing. The results agreed with Simon et al., showing that SBMOF-1 has the highest Xe/Kr selectivity [19]. While SBMOF-1 is a high-performance MOF for Xe/Kr separation, scale up issues arise resulting in low-yield (~50%) [21]. SBMOF-2 was developed by Chen et al. [27] with a Xe/Kr selectivity of 10 and a moderate specific surface area of 195 $m^2 g^{-1}$. They attributed the gas adsorption efficiency to strong -OH polarizing sites pointing into the channels within the sorbent.

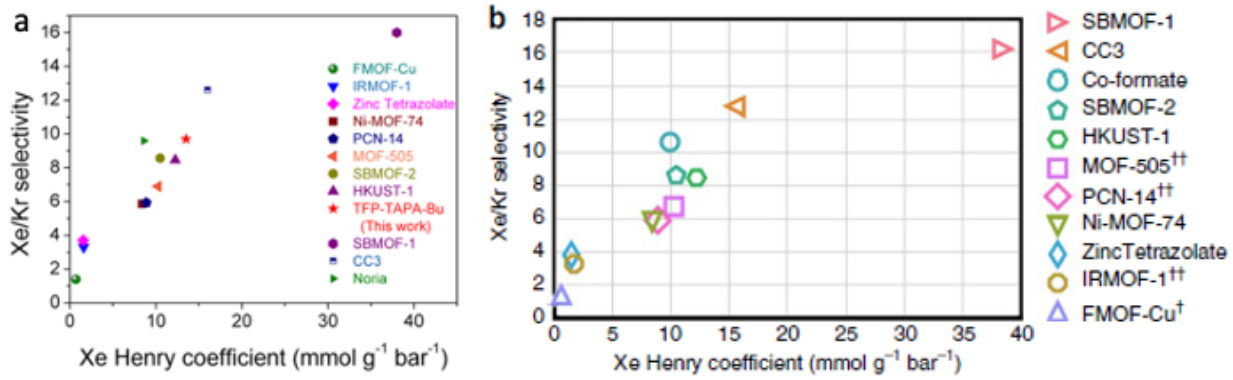

Figure 13. Literature values for Xe/Kr selectivity vs. the Henry coefficient: (a) Jia et al. [28] (b) Banerjee et al. [19]

Continuing the search for structure-property relationships for Xe/Kr selectivities and capacities, Lin et al [29] screened over 320,000 structures in the CoRE MOF, G-MOFs and hMOFs databases and evaluated proposed candidates using datamining techniques. This method found that the assembled *Al_2O_6-fum_B-hmof8* showed the most promise for combined Xe uptake (4.2857 mmol g^1) and Xe/Kr selectivity (19.70) in a 20/80 Xe/Kr mixture [29]. The balance of excellent uptake and selectivity was attributed to the large 1D pore size, which can accommodate a double-atom chain and the large electrostatic potential gradient (EPG) [29].

Several MOFs with OMSs and large pores meet the criteria for potentially excellent adsorption and separation, due to their large surface area and high void fraction. However, OMSs typically exhibit high binding affinity for water, CO_2, and oxygen, and can quickly become saturated in a humid environment [15]. This characteristic does not provide opportunity for robust testing environments; therefore, it is important to study MOFs without OMSs. For example, SBMOF-1 discussed above and the Ni-MOF (chemical formula of $Ni_2^{II}Ni^{III}(\mu_3\text{-}OH)(bdc)_3(tpt)$]) are found to be ideal for this application. The Ni-MOF consists of a window-cage structure, which acts as the only sorption site, and exhibited excellent adsorption capacity during testing [15]. The π-Xe-π structure produces a unique mechanism that enables capture of Xe through van der Waals interactions. Aromatic rings spacing is 4.3 Å compared to the Xe kinetic diameter of 4.047 Å. It has a specific surface area of 884 $m^2 g^{-1}$ with pore size distribution concentrated at 6.8 Å. The isosteric heat of adsorption (Q_{st}) for Xe and Kr were calculated at 25 kJ mol^{-1} and 18.1 kJ mol^{-1}, respectively, indicating a strong preferential adsorption and separation for Xe [15]. Xe uptake is 5.43 mmol g^{-1} and a Henry Xe/Kr selectivity factor was calculated at 7.66 at 298 K and 1 bar.

The calculated IAST selectivity is *ca.* 8.3 at 1 bar. However, no experimental data is available to compare the performance of this MOF with SBMOF-1 under conditions relevant to UNF reprocessing off-gas.

Likewise, another MOF known as MOF Cu-ATC, synthesized by Niu et al. [30] exhibits good Xe and Kr uptake of 5.0 mmol g^{-1} and 2.7 mmol g^{-1} at 298 K and 1 bar and IAST calculated Xe/Kr selectivity of 13.9 at 1 bar. It is also noted that Cu-ATC shows excellent performance characteristics at low pressures (0.1 bar) where Xe and Kr uptakes are reported at 2.65 mmol g^{-1} and 0.52 mmol g^{-1} respectively. PNNL performed Xe and Kr breakthrough experiments in simulated off-gas conditions using Cu-ATC with 400 ppm Xe, and 40 ppm Kr balanced with air at room temperature and compared the Xe capacity with leading MOFs, and porous organic cage materials (Figure 14). The Cu-ATC MOF was found to be the best among all the materials tested at PNNL in terms of Xe capacity and selectivity under reprocessing off-gas mixtures. However, Cu-ATC MOF, was found to compete with CO_2 and water vapor like many of the zeolites and it is difficult to fabricate.

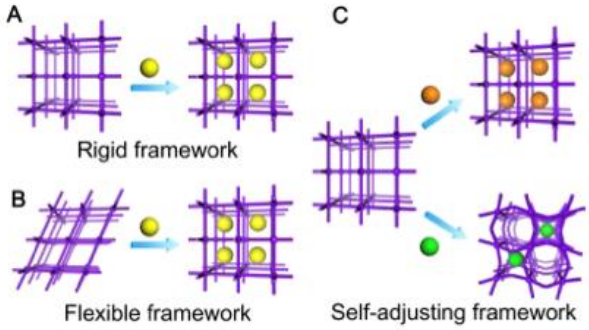

Figure 14. (a) Rigid framework. (b) Flexible framework. (c) Self-adjusting framework. [30]

3.2 Covalent Organic Frameworks

COFs are characterized by a 2D or 3D covalently bonded network, and are formed with light elements such as carbon, hydrogen, oxygen, and nitrogen. They are similar in design to MOFs and zeolites; however, they are composed of non-metal nodes. By adjusting the precursor material and processing conditions, material properties such as porosity and specific surface area can be precisely controlled making them ideal candidates for gas adsorption and separation, which are highly dependent on these properties [28]. Jia et al. found that sub-nanoporous COFs exhibited a maximum adsorption capacity of 85.6 cm^3 g^{-1} for Xe and a Xe/Kr selectivity up to 9.7 at standard temperature and pressure [28]. COFs were prepared via multi-site alkylation of a monomer (1,3,5 trisformylbenzene (TFB) or 1,3,5-triformylphloroglucino (TFB)) with tris(4-aminophenyl)-amine (TAPA). Mid-infrared spectra remained stable for all COFs following 10^5 Gy gamma irradiation.

Another consideration in COF design is organic ligand length. Yuan et al. [31] prepared several materials with varying organic ligand length (Figure 15), and found that TpPa-COF, displayed a higher specific surface area than other materials and thus higher porosity. However, due to the large pore size the adsorption capacities were lower at 1 bar [31].

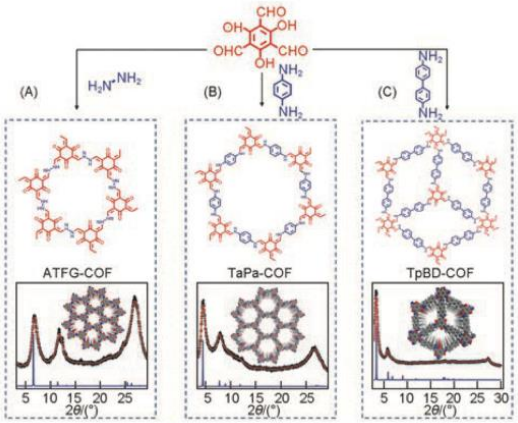

Figure 15. Variation in ligand length and coordination chemistry for (A) ATFG-COF, (B) TaPa-COF, and (C) TpBD-COF. [31]

ATFG-COF is potentially suitable for Xe adsorption as it has a calculated pore size of 0.785 nm with uptakes of 1.72 mmol g^{-1}, 2.21 mmol g^{-1}, and 2.48 mmol g^{-1} at 298 K, 283 K, and 273 K, respectively, at 1 bar pressure [31]. Kr uptakes were lower at 0.54 mmol g^{-1}, 0.69 mmol g^{-1}, and 0.85 mmol g^{-1} at 298 K, 283 K, and 273 K, respectively, at 1 bar pressure. The IAST and Henry's Law Xe/Kr selectivity prediction for ATFG-COF is found to be 6 and 6.07, respectively. Insufficient experimental data exists on COFs under conditions relevant to reprocessing off-gas mixtures.

3.3 Porous Organic Cages and Hydrogen-Bonded Organic Frameworks

Porous organic cages (POCs) and hydrogen-bonded organic frameworks (HOFs) are potential candidates for Xe/Kr separation. Initial investigations into gas separation using HOFs began around 2011 [32-35], with Xe/Kr studies beginning in 2019 [36]. Due to their weak hydrogen bonding, HOFs can be difficult to stabilize; on the other hand, weak bonding can provide additional flexibility for adsorption [32]. Some of the potential advantages of POCs and HOFs include solution processability, easy purification and regeneration by simple recrystallization.

HOF-40, investigated by Gong et al. [37] is an ultra-microporous HOF with a one-dimensional channel and a pore size of 4.15 Å × 3.85 Å. HOF-40 is self-assembled from 1,2,4,5-tetrakis(4-cyanophenyl-benzend) (TCPB). IAST selectivity for X/Kr of 20/80 was calculated to be 11.2 at 298 K and 100 kPa. The Q_{st} was calculated at 32.8 kJ mol^{-1} and 24.4 kJ mol^{-1} for Xe and Kr, respectively, indicating strong preference for Xe absorption. HOF-40 is stable from 12 M HCl to 20 M NaOH. No experimental data exists with reprocessing off-gas mixtures at room temperature.

3.4 Nanoporous Carbons

Other materials such as carbon nanotubes (CNTs) have been investigated for Xe/Kr separation under non-idealized UNF reprocessing off-gas streams which contain additional gaseous byproducts, like I_2 and CH_3I. The Grand Canonical Monte Carlo (GCMC) and Molecular Dynamics (MD) simulations were used for that investigation. In simulated idealized off-gas streams, (6,6) and (7,7) CNTs outperformed other solid sorbents by a factor of 5 and 3, respectively, as seen in Figure 16 [38]. Similar to Banerjee et al. [19], Henry coefficients were used to predict Xe/Kr selectivity and closely match those predicted by GCMC. As compared to the work by Simon et al., the Xe/Kr selectivity was found to increase as the pore size is reduced (Figure 16).

As expected, introducing I_2 and CH_3I into the off-gas stream limits adsorption of Xe as shown in Figure 17 (left). Adsorption of I_2 dominates all but the (6,6) CNT where CH_3I is primarily adsorbed

[38]. It is also useful to note that an ideal pore size may exist to minimize I_2/Xe selectivity. This effect is most pronounced at smaller pore sizes, as depicted in Figure 17 (right) [38]. Additionally, the amorphization of nanoporous carbon hinders the adsorption kinetics.

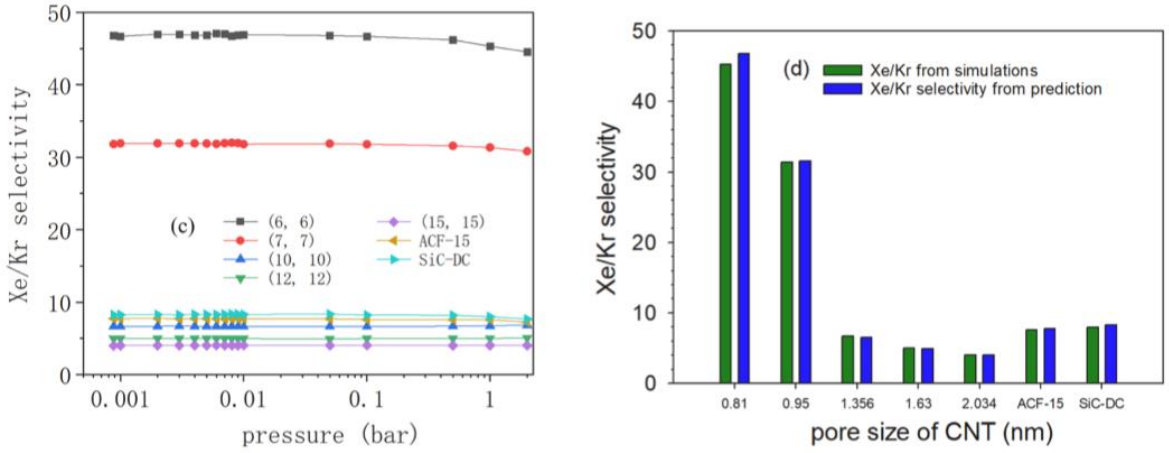

Figure 16. (a) Xe/Kr selectivities as a function of pressure. (b) Xe/Kr selectivity as predicted by Henry constants and calculated based on GCMC simulations at 1.0 bar and 298 K. [38]

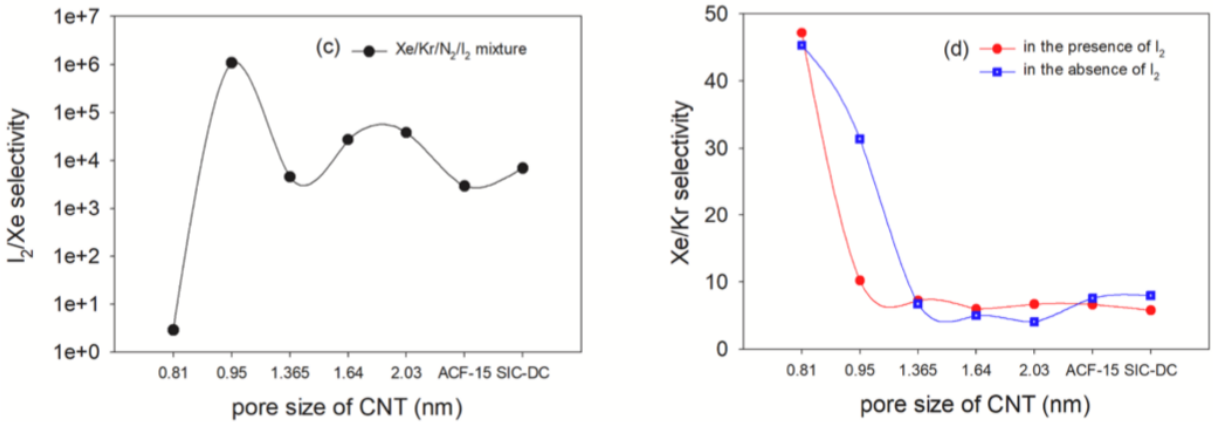

Figure 17. I_2/Xe and Xe/Kr selectivities in different nanoporous carbons. [38]

3.5 Discussion about Engineered Forms

While most of the materials discussed in the literature falling within the categories of MOFs, COFs, POCs, HOFs, and nanoporous solid sorbents are produced in particulate form, engineered forms will be required for implementation in a flowing off-gas stream. Thus, this is an important consideration when selecting a sorbent and matching it with a demonstrated engineered form technology. Some work has been done to convert porous sorbents into engineered forms such as clay binders for zeolites and polymer forms for both zeolites and MOFs [20]. In some cases, solvents used for preparing engineered forms can compromise the functionality of the active ingredient of the sorbent. This is especially true for the water utilized in the polyacrylonitrile (PAN) process used to produce MOF-PAN composites [20], as many MOFs are not compatible with water.

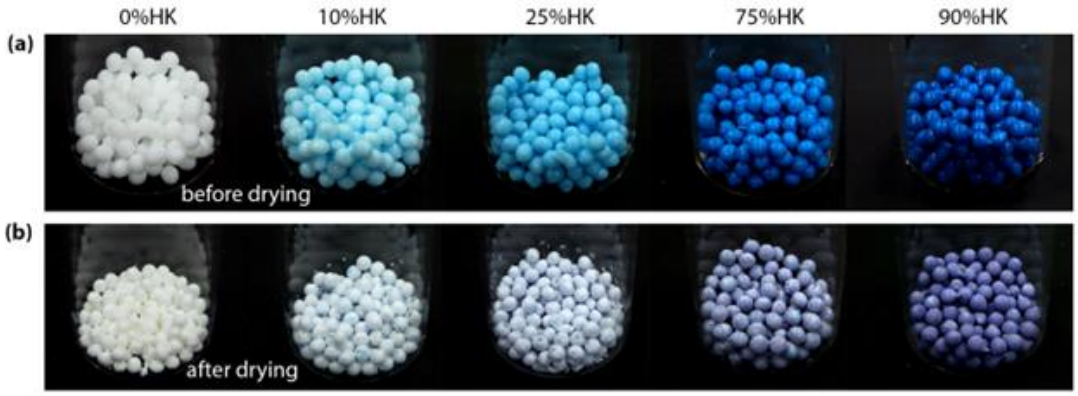

Figure 18. Polyacrylonitrile-MOF composite beads produced with the HKUST-1 MOF before and after drying (for scale, these beads are on the order of 2–3 mm in diameter). This figure was modified from the original by Riley et al. [20].

4. Conclusion

Based on the literature review for sorbents that may outperform AgZ for xenon adsorption, INL and PNNL selected CHA zeolites, ZIF-69, Na-ETS-10, SBMOF-1 (MOF) and CC3(COF) as recommendations for further research. This will include sorbent transformation into an engineering form, preliminary validation testing, and comparable deep bed testing to what was previously conducted on the AgZ sorbent at INL. Testing will be conducted based on the Prioritizing Off-Gas Metrics guide that was drafted at INL in 2023. This report documented a brief history of the respective alternative materials, what testing has been conducted, and what looks promising in outperforming AgZ. For sorbent performance, characteristics such as durability, capacity, room temperature operation, and simplicity were evaluated. These recommendations were based on the research that has already been conducted on the reviewed sorbents and how they compared to research done on AgZ. A comparison of all the sorbents discussed above and AgZ can be seen in Table B1 and Table B2 of Appendix B.

5. References

For quick screening purposes, see Appendix A for accompanying abstracts for these references.

5.1 Zeolite-Based Materials

1. Derbe, T., Temesgen, S., and Bitew, M. 2021. "A Short Review on Synthesis, Characterization, and Applications of Zeolites." *Hindawi*, Article ID 6637898. https://doi.org/10.1155/2021/6637898.
2. Julbe, A. and Drobek, M. 2015. "Zeolite X: Type." *Encyclopedia of Membranes*, p. 1—2. http://dx.doi.org/10.1007/978-3-642-40872-4_607-1.
3. Fomkin, A. A., Serninskii, V.V., and Bering, B.P. 1975. "Investigation of the Adsorption of Xenon on NaX Zeolite Within A Broad Range of Pressures and Temperatures." *Russian Chemical Bulletin*, **24**, 1147–1150. https://doi.org/10.1007/BF00922035.
4. Aristov, B. G., Bosacek, V., and Kiselev, A. V. 1967. "Dependence of Adsorption of Krypton and Xenon by Crystals of Zeolite LiX and NaX on Pressure and Temperature." *Transactions of Faraday Society*, **63**. https://doi.org/10.1039/TF9676302057.
5. Ryoo, R., et al. 1992. "Application of the Xenon-Adsorption Method for the Study of Metal Cluster Formation and Growth on Y Zeolite." *J. Am. Chem. Soc.* **114** (1): 76-82. https://doi.org/10.1021/ja00027a011.
6. Boddenberg, B. and Seidel, A. 1994. "Zinc-exchanged Y Zeolites studied with Carbon Monoxide and Xenon as Probes." *Journal of the Chemical Society, Faraday Transactions*, **9**. https://doi.org/10.1039/FT9949001345.
7. Torcivia, M. A., et al. 2023. "Investigating the Effects of Ag, Cu, and Pd Functionalized Chabazite on the Adsorption Affinities of Noble Gases Xe, Kr, and Ar." *J. Phys. Chem. C*, **127** (7): 3800—3807. https://doi.org/10.1021/acs.jpcc.2c08401.
8. Saxton, C. G., et al. 2009. "Xenon Adsorption in Synthetic Chabazite Zeolites." *Microporous and Mesoporous Materials*, **129** (1-2): 68—73. https://doi.org/10.1016/j.micromeso.2009.08.034.
9. Torkia, Y. B., et al. 2021. Xenon adsorption isotherms on chabazite. Statistical physics modeling investigation: Adsorption energy and pore size distributions computation." *Journal of Environmental Chemical Engineering*, *9* (1): 104733. https://doi.org/10.1016/j.jece.2020.104733.
10. Kuznicki, S. M., et al. 2006. "Xenon Adsorption on Modified ETS-10." *J. Phys. Chem. C*, **111** (4): 1560—1652. https://doi.org/10.1021/jp067630t.
11. Munakata, K., et al. 1999. "Adsorption Equilibria of Krypton, Xenon, Nitrogen and Their Mixtures on Molecular Sieve 5A and Activated Charcoal." *Journal of Nuclear Science and Technology*, **36** (9): 818—829. https://doi.org/10.1080/18811248.1999.9726272.
12. Bazan, R. E., et al. 2011. "Adsorption equilibria of O_2, Ar, Kr, and Xe on activated carbon and zeolites: single component and mixture data." *Adsorption*, **17**, 371—383. https://doi.org/10.1007/s10450-011-9337-3.
13. Luo, S., et al. 2020. "Uptake and separation of Xe and Kr by a zeolitic imidazolate framework with a desirable pore window." *Journal of Radioanalytical and Nuclear Chemistry*, **324** (3). https://link.gale.com/apps/doc/A624275021/AONE?u=anon~ab42ec31&sid=googleScholar&xid=da3041c6.
14. Tsiao, C-j., et al. 1991. "Xenon in Zeolite rho. Adsorption and ^{129}Xenon NMR Spectroscopy." DOI: 0022-3654/91/2095-5586$02.50/0

5.2 Non-Zeolite Based Materials

15. Li, G., et al. 2022. "Efficient and selective capture of xenon over krypton by a window-cage metal–organic framework with parallel aromatic rings." *Separation and Purification Technology*, **295**, 121281. https://doi.org/10.1016/j.seppur.2022.121281.

16. Dorcheh, A. S., et al. 2012. "Noble gases and microporous frameworks; from interaction to application." *Microporous and Mesoporous Materials*, **162**, 64—68. https://doi.org/10.1016/j.micromeso.2012.06.004.

17. Fernandez, C. A., et al. 2012. "Switching Kr/Xe selectivity with temperature in a metal–organic framework." *J. Am. Chem. Soc.*, **134** (22): 9046—9049. https://doi.org/10.1021/ja302071t.

18. Simon, C. M., et al. 2015. "What are the best materials to separate a xenon/krypton mixture?" *Chem. Mater*., **27** (12): 4459—4475. https://doi.org/10.1021/acs.chemmater.5b01475.

19. Banerjee, D., et al. 2016. "Metal–organic framework with optimally selective xenon adsorption and separation." *Nat Commun*, **7**, ncomms11831. https://doi.org/10.1038/ncomms11831.

20. Thallapally, P. K., Grate, J. W., and Motkuri, R.K. 2012. "Facile xenon capture and release at room temperature using a metal–organic framework: a comparison with activated charcoal." *Chemical Communications*, **3**. https://doi.org/10.1039/C1CC14685H.

21. Banerjee, D., Elsaidi, S. K., and Thallapally, P. K. 2017. "Xe adsorption and separation properties of a series of microporous metal–organic frameworks (MOFs) with V-shaped linkers." *J. Mater. Chem. A*, **5**, 16611—16615. https://doi.org/10.1039/C7TA02746J.

22. Mueller, U., et al. 2006. "Metal–organic frameworks—prospective industrial applications." *J. Mater. Chem.*, **16**, 626—636. https://doi.org/10.1039/B511962F.

23. Ryan, P., et al. 2011. "Computational screening of metal-organic frameworks for xenon/krypton separation." *AIChE Journal*, **57** (7): 1759—1766. https://doi.org/10.1002/aic.12397.

24. L. Chen, L. 2014. "Separation of rare gases and chiral molecules by selective binding in porous organic cages." *Nature Mater*, **13**, 954—960. https://doi.org/10.1038/nmat4035.

25. Cooper, E. R., et al. 2004. "Ionic liquids and eutectic mixtures as solvent and template in synthesis of zeolite analogues." *Nature*, **430**, 1012—1016. https://doi.org/10.1038/nature02860.

26. Banerjee, D., et al. 2012. "A calcium coordination framework having permanent porosity and high CO2/N2 selectivity." *Crystal Growth and Design*, **12** (5). https://doi.org/10.1021/cg300274n.

27. Chen, X., et al. 2015. "Direct observation of Xe and Kr adsorption in a Xe-selective microporous metal–organic framework." *J. Am. Chem. Soc.* **137** (22): 7007—7010. https://doi.org/10.1021/jacs.5b02556.

28. Jia, Z. , et al. 2020. "Pore size control via multiple-site alkylation to homogenize sub-nanoporous covalent organic frameworks for efficient sieving of Xenon/Krypton." *ACS Appl. Mater. Interfaces*, **13** (1): 1127—1134. https://doi.org/10.1021/acsami.0c14610.

29. Lin, W.-q., et al. 2023. "Data-mining based assembly of promising metal-organic frameworks on Xe/Kr separation." *Separation and Purification Technology*, **304**, 122357. https://doi.org/10.1016/j.seppur.2022.122357.

30. Niu, Z., et al. 2022. "Self-Adjusting Metal–Organic Framework for Efficient Capture of Trace Xenon and Krypton." *Angewandte Chemie International Edition*, **61** (11). https://doi.org/10.1002/anie.202117807.

31. Yuan, M., et al. 2021. “Tailoring pore structure and morphologies in covalent organic frameworks for Xe/Kr capture and separation.” *Chem. Res. Chin. Univ.*, **37**, 679—685. https://doi.org/10.1007/s40242-021-1064-z.

32. He, Y., Xiang, S., and Chen, B. 2011. “A Microporous Hydrogen-Bonded Organic Framework for Highly Selective C2H2/C2H4 Separation at Ambient Temperature.” *J. Am. Chem. Soc.*, **133** (37): 14570—14573. https://doi.org/10.1021/ja2066016.

33. Li, P., et al. 2015. “A rod-packing microporous hydrogen-bonded organic framework for highly selective separation of C2H2/CO2 at room temperature.” *Angewandte Chemie International Edition*, 54 (2): 574—577. https://doi.org/10.1002/anie.201410077.

34. Li, P., et al. 2014. “A microporous six-fold interpenetrated hydrogen-bonded organic framework for highly selective separation of C 2 H 4/C 2 H 6.” *Chem. Commun.*, **50**, 13081—13084. https://doi.org/10.1039/C4CC05506C.

35. Wang, H., et al. 2015. “A flexible microporous hydrogen-bonded organic framework for gas sorption and separation.” *J. Am. Chem. Soc.*, **137** (31): 9963–9970. https://doi.org/10.1021/jacs.5b05644.

36. Lee, W.-G., et al. 2019. “Selective separation of Xe/Kr and adsorption of water in a microporous hydrogen-bonded organic framework.” *RSC Adv.*, **9** (63): 36808—36814. https://doi.org/10.1039/C9RA08184D.

37. Gong, L., et al. 2022. “A microporous hydrogen-bonded organic framework for efficient Xe/Kr separation.” *ACS Appl. Mater. Interfaces*, **14** (17): 19623–19628. https://doi.org/10.1021/acsami.2c04746.

38. Lin, Z., et al. .2021. “Adsorptive separation of Xe/Kr using nanoporous carbons in the presence of I2 and CH3I.” *Separation and Purification Technology*, **275**, 119161. https://doi.org/10.1016/j.seppur.2021.119161.

39. Xiong, S., et al. 2015. “A flexible zinc tetrazolate framework exhibiting breathing behaviour on xenon adsorption and selective adsorption of xenon over other noble gases.” *J. Mater. Chem. A*, **3** (20): 10747—10752. https://doi.org/10.1039/C5TA00460H.

40. Wang, T., et al. 2020. “Robust bimetallic ultramicroporous metal–organic framework for separation and purification of noble gases.” *Inorg. Chem.*, **59** (7): 4868—4873. https://doi.org/10.1021/acs.inorgchem.0c00134.

41. Banerjee, D., et al. 2018. “Xenon gas separation and storage using metal-organic frameworks.” *Chem.*, **4** (3): 466—494. https://doi.org/10.1016/j.chempr.2017.12.025.

42. Wang, H. 2014. “The first example of commensurate adsorption of atomic gas in a MOF and effective separation of xenon from other noble gases.” *Chem. Sci.*, **5** (2): 620—624. https://doi.org/10.1039/C3SC52348A.

43. Li, L., et al. 2019. “A robust squarate-based metal–organic framework demonstrates record-high affinity and selectivity for xenon over krypton.” *J. Am. Chem. Soc.*, **141** (23): 9358–9364. https://doi.org/10.1021/jacs.9b03422.

44. Mohamed, M. H., et al. 2016. “Hybrid Ultra-Microporous Materials for Selective Xenon Adsorption and Separation.” *Angew Chem Int Ed Engl.*, **55** (29): 8285—9. https://doi.org/10.1002/anie.201602287.

45. Liu, J., Thallapally, P. K., and Strachan, D. 2012. “Metal–organic frameworks for removal of Xe and Kr from nuclear fuel reprocessing plants.” *Langmuir*, **28** (31): 11584—11589. https://doi.org/10.1021/la301870n.

46. Bae, Y.-S., et al. 2013. “High xenon/krypton selectivity in a metal-organic framework with small pores and strong adsorption sites.” *Microporous and Mesoporous Materials*, **169**, 176—179. https://doi.org/10.1016/j.micromeso.2012.11.013.

47. Boutin, A., et al. 2009. “Breathing transitions in MIL-53 (Al) metal–organic framework upon xenon adsorption.” *Angewandte Chemie*, **121** (44): 8464—8467. https://doi.org/10.1002/ange.200903153.

48. Xiong, S., et al. 2018. “A microporous metal–organic framework with commensurate adsorption and highly selective separation of xenon.” *J. Mater. Chem. A*, **6** (11): 4752—4758. https://doi.org/10.1039/C7TA11321H.

49. Chen, R., et al. 2023. “Topology and porosity control on zirconium–fumarate frameworks boosting xenon/krypton separation.” *AIChE Journal*, **69** (10). https://doi.org/10.1002/aic.18169.

Appendix A
Reference Abstracts

Page intentionally left blank

Appendix A

Reference Abstracts

(Ref. 1) The review emphasizes on synthesis, characterization, and application of zeolite. Zeolite is a hydrated aluminosilicate having a tetrahedral structural framework; it contains channels and cages which are occupied by exchangeable active metal ions and water molecules. Zeolite was synthesized through different synthesis methods, particularly, hydrothermal and green synthesis methods. The review also has tried to address the structure of zeolite such as morphology, functional group, and particle size using different characterization methods as reported via different authors. The characterization results verify that zeolite shows many unique properties such as uniform pore size, acidic properties, thermal stability, mobile extra cation, hydrophilicity, and hydrophobicity. These lead to a number of applications in catalysis, water purification, adsorption, and agriculture.

(Ref. 2) Zeolite X, together with zeolite Y, belongs to the family of aluminosilicate molecular sieves with a faujasite-type structure (FAU). It is characterized by the formula $|(Ca, Mg, Na_2)_{29}(H_2O)_{240}|[Al_{58}Si_{134}O_{384}]$– FAU (International zeolite association (IZA)). Faujasite is a rare zeolite, although its synthetic counterparts Linde X and Linde Y are largely used as sorbents and catalysts. Zeolite X differs from zeolite Y by its Si/Al atomic ratio which is typically in the range from 1 to 1.5 for the X and higher for the Y-type zeolite. High Si/Al ratio is desirable towards thermal stability, a property that is less favorable to zeolite X. The 24 tetrahedra cuboctahedral units (sodalite cages) in the FAU framework type are arranged in the same way as the carbon atoms in diamond.

(Ref. 3) A study of the adsorption of freou-13 on NaX zeolite [1-3] in a broad range of pressures p and temperatures T led us to conclusions that are of substantial general practical and theoretical interest. In particular, one of the results of this investigation was the establishment of the linearity of the adsorption isosteres in a plot of logp vs (l/T) within the entire region studied. Moreover, it was found that the isosteres ending at the saturated vapor pressure curve, after a certain break, continue linearly in the region of temperatures above the critical temperature. It seemed interesting to establish the degree of generality of this phenomenon, studying a different system, since the linearity of the isosteres permits a calculation of the adsorption equilibria at high pressures and temperatures on the basis of the experimental data obtained at comparatively low p and T (in a glass apparatus).

(Ref. 4) Adsorption isotherms of xenon on crystals of zeolites LiX and NaX, and krypton on LiX, have been measured at different temperatures. These adsorption isotherms are at first convex towards the gas pressure axis and have an inflection point, while the differential heats of adsorption of xenon and krypton by zeolites increase with increasing adsorption, which is typical for adsorption on a sufficiently homogeneous surface with strong adsorbate-adsorbate attraction. Experimental adsorption isotherms of xenon and krypton on zeolites LiX and NaX are adequately described by simple equations which take approximate account of the interaction of the adsorbed molecules with each other. Temperature dependence of the equilibrium constants of adsorbate-adsorbent and adsorbate-adsorbate of these equations have been determined. These equations make it possible to calculate the adsorption values of xenon and krypton by zeolites LiX and NaX at different gas pressures and temperatures, as well as isosteric heats of adsorption at different adsorption values. The results of these calculations agree with experimental data.

(Ref. 5) Supported metal clusters of **Pt, Ir, Ru, Rh, and Pd** have been prepared in the supercage of Y zeolite by activating their ion-exchanged ammine complexes. Xenon adsorption isotherms obtained from these samples at temperatures ranging from 296 to 340 K and pressures up to 500

Torr, as well as the chemical shift data from the 129Xe NMR study of the adsorbed xenon gas, indicate that the xenon adsorption can occur quite strongly, becoming saturated above ca. 50 Torr, on the metal cluster surface whereas the adsorption is so weak on the support that the adsorbed quantity increases linearly with pressure according to Henry's law.

(Ref. 6) The adsorption isotherms of carbon monoxide and xenon, as well as the ^{129}Xe NMR chemical shifts of xenon, in 55 and 74% zinc-exchanged Y zeolites with various pretreatment conditions, such as temperature of dehydration, oxidation and preloading with CO, have been measured. The sets of experimental data can be explained quantitatively with a unifying approach which considers localized adsorption of both CO and xenon on well-defined adsorption sites consisting of two types of zinc cations in different environments, and sodium cations. The two different zinc cation sites are characterized by their individual adsorption constants and isosteric heats of CO adsorption (63 and 46 KJ mol^{-1}) as well as by the ^{129}Xe NMR chemical shifts of the xenon atoms accommodated on them (185 and 135 ppm). The concentrations of these sites as a function of the degree of zinc exchange and pretreatment conditions were determined.

(Ref. 7) Separation of the noble gases from air is typically done through a cryogenic distillation process that is both energy intensive and expensive. Notably, Ag-functionalized zeolites and MOFs have a well-documented affinity for Xe and, to a lesser extent, Kr that could serve as an economical alternative to this process on a commercial scale. The mechanism driving the Ag–Xe interaction, however, is still a matter of debate, and the use of other metals in place of Ag is not as thoroughly documented. In this study, Ag, Cu, and Pd functionalized chabazite specimens were prepared, and their affinities for the noble gases Xe, Kr, and Ar were investigated and compared to each other and an unexchanged Na-chabazite. From these analyses, Ag-functionalized chabazite displayed the highest affinity for Xe among these samples, but there was not a similar affinity for Kr or Ar. From the results, a mechanism is proposed such that the strong Ag–Xe interaction contains both an underlying physical and electronic aspect related to the formation of Ag nanoclusters within the chabazite pore geometry that alters the chabazite surface state such that Xe is preferentially adsorbed.

(Ref. 8) Xenon adsorption has been studied in different ion-exchanged forms of synthetic chabazite zeolites, K–, Ca–, Li–, Rb– and Cs–CHA, at low pressures and variable temperature. The xenon adsorption capacities vary with the nature of the exchanged cation in a way that is consistent with the known cation locations in the zeolite. Highest uptake was found for Ca–CHA, and lowest for Cs–CHA. The xenon uptakes at room temperature were also consistent with differences in the nitrogen adsorption capacities at 77 K. Enthalpies of adsorption were estimated from the temperature dependence of the adsorption isotherms in Ca–CHA and K–CHA, and found to be very similar. The xenon adsorption was also compared with that of an aluminophosphate (ALPO-CHA) as well as a silicoaluminophosphate (SAPO-34), both having the chabazite-type structure. The high affinity of CHA for xenon is attributed in part to a close match between the size of the xenon atom and the pore dimensions of the CHA structure, the so-called confinement effect.

(Ref. 9) In order to investigate the toxic Xenon removal by an adsorption process on chabazite, the grand canonical formalism of statistical physics has been used. This conducted statistical physics treatment enabled us to draw information about the interactions between Xenon atoms and chabazite surface through the determined physico-chemical parameters. The adsorption energy and pore size distributions have been derived by using an integral expression based on a monolayer model as local isotherm. The fitted values of the steric coefficient showed that one chabazite active site can trap only one Xenon atom. The evaluated densities of receptor sites played an important role in the assess of the adsorption capacity. Ca−CHA sample showed the maximum adsorption capacity (2.36 $mmol.g^{-1}$). By using the adsorption energy distributions (G_D), the physisorbed character of the Xenon adsorption on chabazite samples was brought out.

The diversification of the active sites is noticed for all chabazite samples. The highest adsorption energies are observed in the case of the Xenon adsorption on CA−CHA sample. Furthermore, by using the pore size distribution (PSD), the microporous character of all samples (Ca−CHA, Cs−CHA, Li−CHA, K−CHA and Rb−CHA) has been showed. The maximum surface area was found to be 187.23 m^2. g^{-1} for Ca−CHA. The calculated surface tensions are in the range [10.07E-5 $N.m^{-1}$-13.46E-5 $N.m^{-1}$]. Finally, by combining the thermodynamical and statistical physics treatments, the chemical potential describing the Xenon adsorption, is calculated at different pressures.

(Ref. 10) The interaction of xenon with silver ETS-10 is found to be unusually strong. Xenon adsorption was studied on Na-ETS-10 and its silver exchanged counterpart, Ag-ETS-10, by gas chromatography and gravimetric adsorption. High adsorption capacities were observed even at low pressure (6 wt % Xe at 0.5 Torr and 25 °C). High isosteric heats of adsorption for xenon on Ag-ETS-10 were observed, higher than on any other adsorbent reported to date. High selectivity of xenon over nitrogen and oxygen is also observed, especially at low xenon partial pressures. The great affinity of this adsorbent for xenon is attributed to the presence of silver nanoparticles, which grow on the surface of the molecular sieve after heat treatment of Ag exchanged material.

(Ref. 11) The adsorption equilibria of Kr, Xe and N2, which are constituents of the off-gas from nuclear reprocessing processes, on representative adsorbents (Molecular Sieve 5A (MS5A) and activated charcoal) were studied. Adsorption experiments were conducted in the temperature range of 77 to 323 K using a packed bed column. The adsorption isotherms for the activated charcoal adsorbent were successfully correlated by the vacancy solution model. The adsorption isotherms for the JVIS5A adsorbent were properly correlated by the Langmuir model and the vacancy solution model. The adsorption experiments for the binary component systems (Kr-Xe, Kr-N2 systems) were also performed, and the results suggest that the coexistence of Xe greatly inhibits the adsorption of Kr. The coexistence of large amounts of N2 was also found to inhibit the adsorption of Kr. The experimental results for the adsorption equilibrium of binary component systems on the activated charcoal adsorbent were well reproduced by the vacancy solution model without parameter fitting. The binary adsorption equilibrium on the MS5A adsorbent is rather well predicted by the ideal adsorbed solution model without parameter fitting. The use of the vacancy solution model for this adsorption system requires the optimization of parameters, but the binary adsorption equilibrium is well reproduced with the optimized parameters.

(Ref. 12) This work provides a set of experimental data on the adsorption of pure component, binary and ternary mixtures on activated carbon sample and two different zeolites at 303 K and moderate pressures (up to 10 bar for mixtures). Pure component data were measured by gravimetry and mixture data by volumetry coupled with chromatography. Results encourage more research on new materials and enhancement of adsorption-based separation processes with the proposed target.

(Ref. 13) Crystalline solids of zeolitic imidazolate framework (ZIF)-69 with a suitable pore window size matching with atomic diameter of xenon is utilized for this task, showing notable performance for Xe/Kr capture and separation as well as decent hydrolytic and irradiation stabilities. The results illustrate that the saturated uptake amount of Xe by ZIF-69 is 2.46 mmol/g at 298 K, while Kr uptake is only 0.55 mmol/g. Importantly, the separation ratio of Xe/Kr is 8.35, one of the highest values among all solid sorbent material reported up to now. These findings suggest that ZIF-69 is a potential candidate for the application of xenon capture and purification form a gas mixture containing Kr.

(Ref. 14) The interaction of xenon with zeolite rho is investigated with temperature-dependent adsorption and NMR measurements. From the results, we conclude that xenon can occupy a site at the crystallite surface, as well as sorb into the interior volume. Rapid exchange between these two

sites is detected by the effect on the NMR spectrum. The cesium content of zeolite rho profoundly influences the sorption behavior of xenon. For 0.75 cesium atom/unit cell, q_{iso} = 25 kJ/mol.

(Ref. 15) Efficient capture and separation of xenon (Xe) and krypton (Kr) from nuclear fuel reprocessing plants is of great significance for the control of discharge of gaseous radioisotopes into the environment. However, due to the similar size and chemically inert spherical properties of Xe/Kr, the discovery of an adsorbent with both high adsorption capacity and high selectivity remains a challenge. Here, we report a microporous MOF (Ni-MOF, [Ni2IINiIII(μ3-OH)(bdc)3(tpt)]·guest) featuring two different cavities with an appropriate triangular hole window size. One is composed of parallel aromatic rings with spacings of approximately 4.3 Å comparable to the kinetic diameter of Xe (4.047 Å), affording excellent binding affinity for Xe while the larger one with narrow pore window provides sufficient space for gas adsorption. The Ni-MOF material exhibits an exceptionally high Xe uptake of 5.43 mmol/g and Xe/Kr selectivity of 7.66 at 298 K and 1 bar. The adsorption capacity is the highest among all MOFs without open-metal-sites. Furthermore, the sorption selectivity of Xe over Kr within Ni-MOF originates from a special sandwiched π-Xe-π interaction revealed by Van der Waals interaction calculations.

(Ref. 16) The noble gas storage and separation capability of three classes of microporous frameworks (MFs) including Metal–Organic Frameworks (HKUST-1 and MFU-4l), Covalent-Organic Frameworks (COF-102) and Zeolite Imidazolate Frameworks (ZIF-8) were studied using thermal desorption spectroscopy (TDS). The maxima in the TDS spectra were correlated to the adsorption sites and strength of interactions. The difference in the final desorption temperature for xenon and krypton was correlated to the separation capability of the frameworks. The results show that MFU-4l and HKUST-1 are potential candidates for separation and storage of krypton and xenon. Further sorption studies have proved the ability of both candidates in Kr/Xe separation in larger scale.

(Ref. 17) Krypton (Kr) and xenon (Xe) adsorption on two partially fluorinated metal–organic frameworks (FMOFCu and FMOFZn) with different cavity size and topologies are reported. FMOFCu shows an inversion in sorption selectivity toward Kr at temperatures below 0 °C while FMOFZn does not. The 1D microtubes packed along the (101) direction connected through small bottleneck windows in FMOFCu appear to be the reason for this peculiar behavior. The FMOFCu shows an estimated Kr/Xe selectivity of 36 at 0.1 bar and 203 K.

(Ref. 18) Accelerating progress in the discovery and deployment of advanced nanoporous materials relies on chemical insight and structure–property relationships for rational design. Because of the complexity of this problem, trial-and-error is heavily involved in the laboratory today. A cost-effective route to aid experimental materials discovery is to construct structure models of nanoporous materials in silico and use molecular simulations to rapidly test them and elucidate data-driven guidelines for rational design. For example, highly tunable nanoporous materials have shown promise as adsorbents for separating an industrially relevant gaseous mixture of xenon and krypton. In this work, we characterize, screen, and analyze the Nanoporous Materials Genome, a database of about 670 000 porous material structures, for candidate adsorbents for xenon/krypton separations. For over half a million structures, the computational resources required for a brute-force screening using grand-canonical Monte Carlo simulations of Xe/Kr adsorption are prohibitive. To overcome the computational cost, we used a hybrid approach combining machine learning algorithms (random forests) with molecular simulations. We compared the results from our large-scale screening with simple pore models to rationalize the strong link between pore size and selectivity. With this insight, we then analyzed the anatomy of the binding sites of the most selective materials. These binding sites can be constructed from tubes, pockets, rings, or cages and are often composed of nondiscrete chemical fragments. The complexity of these binding sites emphasizes the importance of high-throughput computational screenings to identify optimal

materials for a given application. Interestingly, our screening study predicts that the two most selective materials in the database are an aluminophosphate zeolite analogue and a calcium based coordination network, both of which have already been synthesized but not yet tested for Xe/Kr separations.

(Ref. 20) Two well-known metal–organic frameworks (MOF-5, NiDOBDC) were synthesized and studied for facile xenon capture and separation. Our results indicate that NiDOBDC adsorbs significantly more xenon than MOF-5, and is more selective for xenon over krypton than activated carbon.

(Ref. 21) A series of microporous metal–organic frameworks (MOFs) constructed by using a V-shaped linker, 4,4′-sulfonyldibenzoic acid, were evaluated for their Xe gas adsorption properties. In particular, a cadmium-based MOF exhibits noteworthy Xe adsorption and separation properties in the presence of other gases under nuclear reprocessing conditions. The outstanding Xe adsorption capacity was attributed to the close pore size matching of the MOF with the kinetic diameter of the Xe atom.

(Ref. 22) The generation of metal–organic framework (MOF) coordination polymers enables the tailoring of novel solids with regular porosity from the micro to nanopore scale. Since the discovery of this new family of nanoporous materials and the concept of so called ‘reticular design’, nowadays several hundred different types of MOF are known. The self assembly of metal ions, which act as coordination centres, linked together with a variety of polyatomic organic bridging ligands, results in tailorable nanoporous host materials as robust solids with high thermal and mechanical stability. Describing examples of different zinc-containing structures, e.g. MOF-2, MOF-5 and IRMOF-8 verified synthesis methods will be given, as well as a totally novel electrochemical approach for transition metal based MOFs will be presented for the first time. With sufficient amounts of sample now being available, the testing of metal–organic frameworks in fields of catalysis and gas processing is exemplified. Report is given on the catalytic activation of alkynes (formation of methoxypropene from propyne, vinylester synthesis from acetylene). Removal of impurities in natural gas (traces of tetrahydrothiophene in methane), pressure swing separation of rare gases (krypton and xenon) and storage of hydrogen (3.3 wt% at 2.0 MPa/77 K on Cu-BTC-MOF) will underline the prospective future industrial use of metal-organic frameworks in gas processing. Whenever possible, comparison is made to state-of-art applications in order to outline possibilities which might be superior by using MOFs.

(Ref. 23) A variety of metal-organic frameworks (MOFs) with varying linkers, topologies, pore sizes, and metal atoms were screened for xenon/krypton separation using grand canonical Monte Carlo (GCMC) simulations. The results indicate that small pores with strong adsorption sites are desired to preferentially adsorb xenon over krypton in multicomponent adsorption. However, if the pore size is too small, it can significantly limit overall gas uptake, which is undesirable. Based on our simulations, MOF-505 was identified as a promising material due to its increased xenon selectivity over a wider pressure range compared with other MOFs investigated.

(Ref. 24) The separation of molecules with similar size and shape is an important technological challenge. For example, rare gases can pose either an economic opportunity or an environmental hazard and there is a need to separate these spherical molecules selectively at low concentrations in air. Likewise, chiral molecules are important building blocks for pharmaceuticals, but chiral enantiomers, by definition, have identical size and shape, and their separation can be challenging. Here we show that a porous organic cage molecule has unprecedented performance in the solid state for the separation of rare gases, such as krypton and xenon. The selectivity arises from a precise size match between the rare gas and the organic cage cavity, as predicted by molecular simulations. Breakthrough experiments demonstrate real practical potential for the separation of krypton, xenon and radon from air at concentrations of only a few parts per million. We also

demonstrate selective binding of chiral organic molecules such as 1-phenylethanol, suggesting applications in enantioselective separation.

(Ref. 25) The challenges associated with synthesizing porous materials1 mean that new classes of zeolites (zeotypes)—such as aluminosilicate zeolites2,3 and zeolite analogues4—together with new methods of preparing known zeotypes5, continue to be of great importance. Normally these materials are prepared hydrothermally with water as the solvent in a sealed autoclave under autogenous pressure6. The reaction mixture usually includes an organic template or 'structure-directing agent' that guides the synthesis pathway towards particular structures. Here we report the preparation of aluminophosphate zeolite analogues by using ionic liquids7 and eutectic mixtures8. An imidazolium-based ionic liquid acts as both solvent and template, leading to four zeotype frameworks under different experimental conditions. The structural characteristics of the materials can be traced back to the solvent chemistry used. Because of the vanishingly low vapour pressure of ionic liquids, synthesis takes place at ambient pressure, eliminating safety concerns associated with high hydrothermal pressures. The ionic liquid can also be recycled for further use. A choline chloride/urea eutectic mixture8 is also used in the preparation of a new zeotype framework.

(Ref. 26) A thermally stable, microporous calcium coordination network shows a reversible 5.75 wt % CO2 uptake at 273 K and 1 atm pressure, with an enthalpy of interaction of ~31 kJ/mol and a CO2/N2 selectivity over 45 under ideal flue gas conditions. The absence of open metal sites in the activated material suggests a different mechanism for selectivity and high interaction energy compared to those for frameworks with open metal sites.

(Ref. 27) The cryogenic separation of noble gases is energy-intensive and expensive, especially when low concentrations are involved. Metal–organic frameworks (MOFs) containing polarizing groups within their pore spaces are predicted to be efficient Xe/Kr solid-state adsorbents, but no experimental insights into the nature of the Xe–network interaction are available to date. Here we report a new microporous MOF (designated SBMOF-2) that is selective toward Xe over Kr under ambient conditions, with a Xe/Kr selectivity of about 10 and a Xe capacity of 27.07 wt % at 298 K. Single-crystal diffraction results show that the Xe selectivity may be attributed to the specific geometry of the pores, forming cages built with phenyl rings and enriched with polar -OH groups, both of which serve as strong adsorption sites for polarizable Xe gas. The Xe/Kr separation in SBMOF-2 was investigated with experimental and computational breakthrough methods. These experiments showed that Kr broke through the column first, followed by Xe, which confirmed that SBMOF-2 has a real practical potential for separating Xe from Kr. Calculations showed that the capacity and adsorption selectivity of SBMOF-2 are comparable to those of the best-performing unmodified MOFs such as NiMOF-74 or Co formate.

(Ref. 28) Among various fission products generated in nuclear reactors, xenon and krypton are two important fission gases with high flow, diffusivity, and radioactivity. Moreover, xenon isolated from these products is an expensive industrial resource with wide applications in medicine and lighting, which makes the development of efficient methods for separation of xenon/krypton significant. However, it is usually difficult for xenon/krypton to be adsorbed by chemical adsorbents due to their inert gas properties, and sub-nanoporous adsorbents proven to be workable for the separation of xenon/krypton are still hard to prepare and regulate the pore size. Herein, we report two novel sub-nanoporous covalent organic frameworks (COFs), which were applied to the sieving of xenon/krypton for the first time. The sub-nanoporous COFs were synthesized via aldehyde–amine polycondensation reactions and the subsequent pore size regulation and homogenization process by using a facile, operational, and efficient multiple-site alkylation strategy. Impressively, the as-prepared sub-nanoporous COFs realized the efficient adsorption and sieving of xenon/krypton owing to their slightly larger pore sizes (~7 Å) than the dynamic diameters of xenon/krypton and their larger pore volumes. The maximum adsorption

capacity for xenon is up to 85.6 cm3/g, and the xenon/krypton selectivity can reach to 9.7. Moreover, the as-prepared COFs possess good γ-ray irradiation stability, which endows them with great potentials for the sieving of radioactive xenon/krypton in the practical application. The multiple-site alkylation strategy proposed in this study provides a valuable approach for the pore construction and control of the porous materials, especially the sub-nanoporous adsorption materials.

(Ref. 29) The adsorptive separation of xenon (Xe) and krypton (Kr) becomes increasingly important for the treatment of used nuclear fuel (UNF), and thus the novel high-performing metal-organic frameworks (MOFs) on Xe/Kr adsorption separation are urgently needed. In this work, the 200 MOFs formally used for ethane/ethylene separation were adapted to construct structure-adsorption property relationships (SAPR) for Xe/Kr mixture (20/80 v/v) at 298 K and 1 bar, to screen for MOFs with large Xe/Kr selectivities and Xe uptakes in the CoRE MOF, G-MOFs and hMOFs databases with more than 320,000 structures. Then based on the screened 1499 MOFs, the important metal nodes and organic linkers of MOFs (genes) governing the Xe uptake were identified by data-mining of feature engineering, which were assembled crossly into three novel promising MOFs according to material genomics strategy. After considering of the regenerabilities, it is found that Xe uptake (4.2857 mmol/g) and Xe/Kr selectivity (19.70) of the assembled Al2O6-fum_B-hmof8_No1 are larger than those of the most of experimentally synthesized frameworks including Al-Fum-Me, overcoming the “trade-off” problem between adsorption selectivity and capacity. From the multiscale calculations at GCMC and DFT levels, it is found that the large 1D pore size that can accommodate a double-atom chain and large electrostatic potential gradient (EPG) should be responsible for the high Xe uptake and Xe/Kr selectivity of Al2O6-fum_B-hmof8_No1, respectively. Note that the present work first report double-atom chain of rare gas adsorbed in MOF materials. The present data mining and cross assembly strategies are expected to assist the discovery of novel high-performing MOF absorbents for the separation of Xe-Kr even light hydrocarbon in the future.

(Ref. 30) The capture of the xenon and krypton from nuclear reprocessing off-gas is essential to the treatment of radioactive waste. Although various porous materials have been employed to capture Xe and Kr, the development of high-performance adsorbents capable of trapping Xe/Kr at very low partial pressure as in the nuclear reprocessing off-gas conditions remains challenging. Herein, we report a self-adjusting metal-organic framework based on multiple weak binding interactions to capture trace Xe and Kr from the nuclear reprocessing off-gas. The self-adjusting behavior of ATC-Cu and its mechanism have been visualized by the in-situ single-crystal X-ray diffraction studies and theoretical calculations. The self-adjusting behavior endows ATC-Cu unprecedented uptake capacities of 2.65 and 0.52 mmol g−1 for Xe and Kr respectively at 0.1 bar and 298 K, as well as the record Xe capture capability from the nuclear reprocessing off-gas. Our work not only provides a benchmark Xe adsorbent but proposes a new route to construct smart materials for efficient separations.

(Ref. 31) As a rising star among porous solid materials, covalent organic frameworks(COFs) with excellent properties including but not limit to facilely controllable structure, high porosity, and multi-chemical functionality represent significant potential for efficient 127Xe/85Kr capture and separation. In this study, through tuning the length of the organic ligands, two-dimensional(2D) COF materials with identical connection group but different pore properties, denoted as ATFG-COF and TpPa-COF with AA-stacking model and TpBD-COF with AB-stacking model were synthesized and tested for Kr and Xe adsorption for the first time. Adsorption measurements indicate that the narrower pore apertures and higher porosity are conducive for COF materials to capture Xe and Kr. Furthermore, the Henry’s constant, isosteric heat of adsorption(Qst), and ideal adsorbed solution theory(IAST) selectivity of ATFG-COF, the pore size of which is closest to the kinetic diameter of the Xe atom(0.41 nm) among 2D COF materials, were carried out based on

the single component sorption isotherms. The results illustrate that the high isosteric heat values of Xe/Kr adsorption on ATFG-COF are 25 and 16 kJ/mol at room temperature, respectively. Henry's law predicts that the selectivity factor of Xe to Kr is 6.07, consistent with the adsorption selectivity(ca. 6) calculated based on the IAST.

(Ref. 37) Separation of xenon/krypton gas mixtures is one of the valuable but challenging processes in the gas industries due to their close molecular size and similar physical properties. Here, we report a novel ultramicroporous hydrogen-bonded organic framework (termed as HOF-40) constructed from a cyano-based organic building unit of 1,2,4,5-tetrakis(4-cyanophenyl)benzene (TCPB), exhibiting superior separation performance for Xe/Kr mixtures, as clearly demonstrated by dynamic breakthrough curves. GCMC simulation results indicate that the pore confinement effect and abundant accessible binding sites play a synergistic role in this challenging gas separation. Furthermore, this cyano-based HOF displays excellent chemical stability from 12 M HCl to 20 M NaOH aqueous solutions.

(Ref. 38) Grand canonical Monte Carlo (GCMC) and molecular dynamic (MD) simulations were systematically conducted to reveal the influence of volatile radionuclides, I2 and CH3I, on the adsorption of Xe/Kr/N2 mixtures in well-shaped carbon nanotubes (CNTs), stratified activated carbon fiber (ACF-15) and completely disordered silicon carbide derived carbon (SiC-DC). In the absence of radioactive impurities, the (6, 6) CNT with a pore size of 0.81 nm achieves adequately high adsorption of Xe (0.37 mol/kg) and Xe/Kr selectivity (45.3), presenting significantly superior performance than other CNTs and amorphous carbons. Albeit enhancing the amorphization of nanoporous carbons hardly impacts the sorption capacity, it hinders the adsorption kinetics dramatically by introducing the energy barriers to diffusion. However, when either I2 or CH3I presents in the gas phase, the adsorptions of Xe and Kr are severely excluded in nanoporous carbons due to the dominant adsorption of I2 and CH3I. For the Xe/Kr/N2/I2/CH3I mixture, the intense competitive adsorption occurs between I2 and CH3I in nanoporous carbons. It is found while the (6, 6) CNT demonstrates the greatest potential on separating CH3I from the quinary mixture, the (15, 15) CNT achieves the best performance on separating I2 among the carbon structures considered.

(Ref. 39) Given the fact that traditional cryogenic rectification is highly energy and capital intensive for the purification of xenon, effective selective adsorption of xenon over other noble gases at room temperature using porous materials is a critical and urgent issue. Here, we present a flexible zinc tetrazolate framework ([Zn(mtz)2]), which exhibits a high capture capacity for xenon and selective adsorption of xenon over other noble gases at room temperature. Due to its high adsorption enthalpy for xenon, a suitable pore size that matches well with the xenon atom, as well as the high polarizability of Xe, [Zn(mtz)2] shows breathing behaviour on xenon adsorption, which is confirmed by the experimental adsorption isotherms of xenon and thermodynamic analysis of breathing transition. The isosteric heats of adsorption and S(DIH) calculations indicate that [Zn(mtz)2] has significantly higher adsorption affinity and capacity for Xe compared with Kr, Ar and N2. The high capture capacity of Xe (2.7 mmol g−1) in an idealized PSA process and high Xe/Kr selectivity (15.5) from breakthrough experiment promise the potential application of [Zn(mtz)2] in Xe capture and separation from Xe–Kr gas mixtures.

(Ref. 40) Noble gases, especially krypton (Kr) and xenon (Xe), are widely applied in diverse fields. Developing new techniques and adsorbents to separate and purify Kr and Xe is in high demand. Herein, we reported a bimetallic metal–organic framework (MOF) (NKMOF-1-Ni) which possesses a narrow pore size (5.36 Å) and ultrahigh stability (e.g., stable in water for 1.5 years). Gas sorption measurements revealed that this MOF possessed much higher uptake for Xe than for Kr, Ar, or N2 at room temperature in all pressure ranges. The calculation of adsorption isosteric heat and Grand Canonical Monte Carlo simulation verified that NKMOF-1-Ni had a stronger interaction with Xe than other tested gases. The results of ideal adsorbed solution theory

selectivity and simulated breakthrough further showed that NKMOF-1-Ni had an outstanding separation performance of Xe/Kr, Xe/Ar, and Xe/N2. This study provides important guidance for future research to synthesize ideal sorbents to separate noble gases.

(Ref. 41) The global demand for Xenon (Xe), a noble gas with applications in electronics, lighting, and the medical industry, is expected to increase significantly over the coming decades. However, the low abundance of Xe in the Earth's atmosphere and the costly cryogenic distillation process that is used to obtain Xe commercially via air separation have limited the scale of applications of Xe. A physisorption-based separation using porous materials could be a viable and cost-effective alternative to cryogenic distillation. In particular, metalorganic frameworks (MOFs) have shown promise as highly Xe-selective porous solids. In this review, we discuss the recent advances of MOFs as adsorbents for noble gas adsorption and separation and the role of computer simulation in finding optimal materials for Xe adsorption.

(Ref. 42) In industry, cryogenic rectification for separating xenon from other noble gases such as krypton and argon is an energy and capital intensive process. Here we show that a microporous metal-organic framework, namely Co3(HCOO)6 is capable of effective capture and separation of xenon from other noble gases. Henry's constant, isosteric heat of adsorption (Qst), and IAST selectivity are calculated based on single component sorption isotherms. Having the highest Qst reported to date, Co3(HCOO)6 demonstrates high adsorption capacity for xenon and its IAST selectivity for Xe-Kr is the largest among all MOFs investigated to date. To mimic real world conditions, breakthrough experiments are conducted on Xe–Kr binary mixtures at room temperature and 1 atmosphere. The results are consistent with the calculated data. These findings show that Co3(HCOO)6 is a promising candidate for xenon capture and purification. Our gas adsorption measurements and molecular simulation study also reveal that the adsorption of xenon represents the first example of commensurate adsorption of atomic gases near ambient conditions.

(Ref. 43) The efficient separation of xenon (Xe) and krypton (Kr) is one of the industrially important processes. While adsorptive separation of these two species is considered to be an energy efficient process, developing highly selective adsorbent remains challenging. Herein, a rigid squarate-based metal–organic framework (MOF), having a perfect pore size (4.1 Å × 4.3 Å) comparable with the kinetic diameter of Xe (4.047 Å) as well as pore surface decorated with very polar hydroxyl groups, is able to effectively discriminate Xe atoms, affording a record-high Xe/Kr selectivity. An exceptionally high Xe uptake capacity of 58.4 cm3/cm3 and selectivity of 60.6 at low pressure (0.2 bar) are achieved at ambient temperature. The MOF exhibits the highest Xe Henry coefficient (192.1 mmol/g/bar) and Xe/Kr Henry selectivity (54.1) among all state-of-the-art adsorbents reported so far. Direct breakthrough experiments further confirm the excellent separation performance. The density functional theory calculations reveal that the strong interaction between Xe and the framework is a result of the synergy between optimal pore size and polar porosity.

(Ref. 44) The demand for Xe/Kr separation continues to grow due to the industrial significance of high-purity Xe gas. Current separation processes rely on energy intensive cryogenic distillation. Therefore, less energy intensive alternatives, such as physisorptive separation, using porous materials, are required. Herein we show that an underexplored class of porous materials called hybrid ultra-microporous materials (HUMs) affords new benchmark selectivity for Xe separation from Xe/Kr mixtures. The isostructural materials, CROFOUR-1-Ni and CROFOUR-2-Ni, are coordination networks that have coordinatively saturated metal centers and two distinct types of micropores, one of which is lined by CrO_4^{2-} (CROFOUR) anions and the other is decorated by the functionalized organic linker. These nets offer unprecedented selectivity towards Xe. Modelling indicates that the selectivity of these nets is tailored by synergy between the pore size and the strong electrostatics afforded by the CrO_4^{2-} anions.

(Ref. 45) Removal of xenon (Xe) and krypton (Kr) from process off-gases containing 400 ppm Xe, 40 ppm Kr, 78% N2, 21% O2, 0.9% Ar, 0.03% CO2, and so forth using adsorption was demonstrated for the first time. Two well-known metal–organic frameworks (MOFs), HKUST-1 and Ni/DOBDC, which both have unsaturated metal centers but different pore morphologies, were selected as novel adsorbents. Results of an activated carbon were also included for comparison. The Ni/DOBDC has higher Xe/Kr selectivities than those of the activated carbon and the HKUST-1. In addition, results show that the Ni/DOBDC and HKUST-1 can adsorb substantial amounts of Xe and Kr even when they are mixed in air. Moreover, the Ni/DOBDC can successfully separate 400 ppm Xe from 40 ppm Kr and air containing O2, N2, and CO2 with a Xe/Ke selectivity of 7.3 as indicated by our breakthrough results. This shows a promising future for MOFs in radioactive nuclide separations from spent fuels.

(Ref. 46) Separation of Xe/Kr mixtures was studied in two copper-paddlewheel metal-organic framework materials, MOF-505 and HKUST-1. For MOF-505, which has small pores with strong adsorption sites, high Xe/Kr selectivities (9–10) are obtained from breakthrough measurements and grand canonical Monte Carlo (GCMC) simulations. The consistent results from both techniques suggest that MOF-505 is a promising candidate for Xe/Kr separation. For HKUST-1, which has small octahedral pores, only modest Xe/Kr selectivities (4.5) are observed from breakthrough measurements, although the GCMC simulations predicted unusually high selectivities at low loadings.

(Ref. 47) Die Auswertung temperaturabhängiger Adsorptionsexperimente im Rahmen eines thermodynamischen Osmose-Modells führt zu einem T-p-Phasendiagramm, das ein ungewöhnliches Aus- und Eintrittsverhalten der Gasmoleküle offenbart. Der beobachtete Atmungseffekt im metall-organischen Gerüst MIL-53(Al) scheint ein allgemeines Phänomen zu sein, das in einem begrenzten Temperaturbereich unabhängig vom Adsorbat auftreten sollte.

(Ref. 48) The separation of xenon (Xe) and krypton (Kr) becomes increasingly important due to the industrial significance of high-purity Xe gas and the concern with reprocessing radioactive isotopes of Xe and Kr at parts per million concentrations from the off-gas of used nuclear fuel. Current separation processes mainly rely on energy and capital intensive cryogenic distillation. Thus, more economical and energy-efficient alternatives, such as physisorptive separation, using porous materials are needed to be developed. Herein, we present a microporous metal–organic framework (MOF-Cu-H) in which the suitable pore/cage-like structure with a precise size matching with the xenon atom leads to its commensurate adsorption phenomenon of Xe under ambient conditions and superior performance for Xe capture and separation. MOF-Cu-H exhibits by far the highest Xe Henry coefficient, remarkable Xe/Kr selectivity and significantly high Xe adsorption capacity at very low partial pressures relevant to nuclear fuel reprocessing. Temperature dependent isotherms, adsorption kinetics experiments, single column breakthrough curves and molecular simulation studies collaboratively support the claim, underlining the potential of this material for energy and cost-effective removal of xenon from nuclear fuel reprocessing plants compared with cryogenic distillation.

(Ref. 49) The designability and ultrahigh stability of zirconium–organic frameworks make them attractive adsorbents for noble gases xenon (Xe) and krypton (Kr), but their Xe/Kr separation performance needs to be further enhanced. In this study, we rationally control the topology and porosity of zirconium–fumarate frameworks by simply changing the synthesis conditions, and successfully construct an adsorbent (named as MIP-203-F) with one-dimensional pore instead of the original cage-like fcu metal–organic framework MOF-801. The Xe/Kr separation performance of MIP-203-F is thoroughly evaluated by isotherm measurements and breakthrough experiments, while the adsorption mechanism is elucidated in detail by Monte Carlo and density functional theory calculations. Due to the uniform pore with suitable size and abundant polarization groups,

MIP-203-F can differentially polarize and recognize atomic Xe/Kr gases, and establishes a new record among zirconium–organic frameworks for the capture and separation of Xe/Kr.

Appendix B
Alternative Materials Reference Tables

Page intentionally left blank

Appendix B
Alternative Materials Reference Tables

Table B1. Literature review of selected zeolite-based materials for Xe capture.

Material	Testing Form	How is it aquired?	Surface Area (m^2/g)	Average Pore Size (nm)	Pore Volume (cm^3/g)	Temperature [K]	Gas Concentration	Flowrate	Amount of Material Tested	Xenon Capacity	Xe/Kr Selectivity	Xe/N_2 Selectivity	Henry's Law Constants	Reference
NaX	Bead	Synthesized	—	—	—	150, 165, 180, 210, 240, 280, 296, 310, 330, 350, 370	Pure Xe	—	—	150 mmol/kg	—	—	—	[3]
NaX	Bead	Synthesized	—	—	—	183, 193, 198, 213, 228, 243	—	—	—	5.3 mmol/g	—	—	—	[4]
LiX	Bead	Synthesized	—	—	—		—	—	—	6.1 mmol/g	—	—	—	
NaY	Bead	Synthesized	—	—	—	296 and 310	Pure Xe	—	—	—	—	—	—	[5]
Pt/NaY	Bead	Synthesized	—	—	—			—	—	—	—	—	—	
Ru/NaY	Bead	Synthesized	—	—	—			—	—	—	—	—	—	
NaY	Bead	Synthesized	—	—	—	273-309	Pure Xe	—	—	—	—	—	—	[6]
Zn(55)Y	Bead	Synthesized	—	—	—			—	—	—	—	—	—	
Zn(74)Y	Bead	Synthesized	—	—	—			—	—	—	—	—	—	
CHA	Bead	Commercial	466	—	0.231	373, 398, 423, 448, 463, 473	40 uL of test gas (Kr, Xe, Ar)	10.8 mL/min	~ 2 g	—	—	—	—	[7]
Cu-CHA	Bead	Commercial	460	—	0.231					—	—	—	—	
Pd-CHA	Bead	Commercial	422	—	0.218					—	—	—	—	
K-CHA	Bead	Synthesized	-	—	0.005	197-318	—	—	0.1 g	—	—	—	—	[8]
Ca-CHA	Bead	Commercial	187.23	3.0-18.0	—	298	—	—	0.1 g	2.36 mmol/g	—	—	—	[9]
Cs-CHA	Bead	Commercial	14.28	5.0-14.0	—		—	—		0.18 mmol/g	—	—	—	
Rb-CHA	Bead	Commercial	85.68	6.0-10.0	—		—	—		1.08 mmol/g	—	—	—	
K-CHA	Bead	Commercial	149.94	3.8-19.6	—		—	—		1.89 mmol/g	—	—	—	
Li-CHA	Bead	Commercial	150.74	4.0-20.0	—		—	—		1.9 mmol/g	—	—	—	

Material	Testing Form	How is it aquired?	Surface Area (m^2/g)	Average Pore Size (nm)	Pore Volume (cm^3/g)	Temperature [K]	Gas Concentration	Flowrate	Amount of Material Tested	Xenon Capacity	Xe/Kr Selectivity	Xe/N_2 Selectivity	Henry's Law Constants	Reference
Na-ETS-10	Bead	Synthesized	—	—	—	303, 325, 343, 373	Pure Xe, N_2, and O_2	—	—	—	—	13-18	—	[10]
Molecular Sieve 5A	Bead	Commercial	415	—	—	353, 323, 303, 273, 195, 159, 77	Pure Kr, Xe, and N_2 and Binary Mixture (Xe and Kr)	1.65-36.7 cm^3/s	2.1-280 g	—	—	—	—	[11]
Koestrolith 13X-K2	Bead	Commercial	640	0.9	0.356	303	Pure gas (O_2, Ar, Kr, Xe) and Mixed Gas (Kr/Ar, Xe/Ar, Xe/Kr, O2/Ar, Kr/O2, Xe/O2)	—	—	11.344 mmol/g	—	—	—	[12]
Koestrolith 4K	Bead	Commercial	477	0.4	0.198			—	—	3.918 mmol/g	—	—	—	
ZIF-69	Crystals	Commercial	—	—	—	273, 283, 293, 298	Pure gas (Kr and Xe)	—	—	2.46, 3.14, 2.56 mmol/g	8.35 @ 298 K	—	5.9321 @ 298K	[13]
Zeolite Rho	Bead	Commercial	—	—	—	195, 225, 245, 273, 300	Pure Xe	—	0.5 g	—	—	—	—	[14]

Table B2. Reviewed alternative materials for xenon capture. All data were collected or calculated at 298 K, 1 bar, unless otherwise stated.

Material	Class	How is it acquired?	SSA (m^2g^1)	Pore Size (Å)	Henry Selectivity 1 bar (Xe/Kr)	Henry Selectivity 1 bar (Xe/Kr)	Breakthrough Selectivity 1 bar (Xe/Kr)	Xe uptake 1 bar, 298 K (mmol kg^{-1})	Reference
$[Zn(tmz)_2]$	MOF	-	-	-	-	-	15.5[b]	2.7[b,k]	[27]
Ag-MOF-303	MOF	-	716	5.2	-	10.4[a] (0.2 bar)	-	5.9[a,k] (0.2 bar)	[28]
Cu-ATC	MOF	-	600	6.24	-	13.9[a]	-	32[j]	[16]
ATFG-COF	COF	-	244	7.85	-	6[a]	-	1.72[a,k]	[17]
Carbon-Z	Carbon	-	-	-	-	-	-	3.17[e,k]	[29]
Carbon-ZX	Carbon	-	-	-	-	-	-	4.42[e,k]	[29]
CC3	POC	-	-	4.4	-	-	20.4[d]	11[d]	[10]
CNT (6,6)	Carbon	-	-	8.1	45.3[i]	-	-	0.37[i,k]	[24]
Co-formate ($Co_3(HCOO)_6$)	MOF	-	300	5	-	12[e]	6[c]	2.0[e,k]	[30]
Co-squrate	MOF	-	95	4.1	51.4[e]	69.7[a]	-	-	[31]
CROFOUR-1-Ni	HUMM	-	-	-	-	21.5[c], 22[a], 26[b],	19.8[a]	1.8[a,k]	[32]
CROFOUR-2-Ni	HUMM	-	475	-	-	15[c], 15.5[a], 16[b]	14.3[a]	1.6[a,k]	[32]
FMOF-Cu	MOF	Synthesized	56.39	-	-	-	2[e]	-	[3]
HKUST-1	OMS	Commercial	1710	-	11.8[e] (280 K), 8.4[e]	-	3[d], 2.6[a], 5[a]	8.5[a]	[2, 33-35]
HOF-40	POC	-	234	-	-	11.2[a]	-	-	[23]
MFU-4l	MOF	Synthesized	3500	4.15 x 3.85	5.6	-	-	-	[2]
MIL-53-Al	MOF	Commercial	1300	-	-	-	-	-	[36]
MOF-5	MOF	-	3400	-	-	-	-	1.98[k]	[6, 33]
MOF-505	MOF	-	1030	4.8	-	9-10[a]	8[a]	6.31[a,k]	[9, 35]
MOF-74 Mg	MOF	-	-	-	-	-	5.92	5.58[k]	[33]
MOF-Cu-H	MOF	-	-	-	15.8	16.7[a]	-	13[f], 3.19[a,k]	[1, 37]

Material	Class	How is it acquired?	SSA (m^2g^1)	Pore Size (Å)	Henry Selectivity 1 bar (Xe/Kr)	Henry Selectivity 1 bar (Xe/Kr)	Breakthrough Selectivity 1 bar (Xe/Kr)	Xe uptake 1 bar, 298 K (mmol kg^{-1})	Reference
Ni-MOF	MOF	-	884	4.3	7.66	8.3	-	5.43 [a,k]	[1]
Ni-MOF-74	MOF	-	-	-	-	5-6[d], 7.3[a]	-	4.8[d], 4.19[a,k]	[33]
NiDOBDC	OMS	-	950	-	-	-	7.3[d]	9.3[g]	[34]
NKMOF-1-Ni	MOF	-	354	5.36	-	5.2[a]	-	2.28[a,k,l]	[38]
Noria	POC	-	-	5 -7	-	-	9.4[d]	1.55[e,k]	[33]
SBMOF-1	MOF	-	-	-	16[d]	-	16[a]	13.2[d], 1.38[a,k]	[5, 33]
SBMOF-2	MOF	-	195	-	-	10[a]	-	0.8[h,k]	[13, 33]
TpBD-COF	COF	-	226	-	-	-	-	7.3[e,k]	[17]
TpPa-COF	COF	-	587	-	-	-	-	1.5[e,k]	[17]
UiO-66	MOF	Commercial	1660	-	-	5.9[a]	-	-	[39]
MOF-801	MOF	Commercial	946	6.7a	-	7.6[a]	-	-	[39]
MIP-203-F	MOF	Synthesized	-	-	9.1[e]	-	-	7.9[d]	[39]
MOF-303	MOF	Commercial	-	-	-	-	-	-	-
MIL-100(Fe)	MOF	Commercial	-	-	-	-	-	-	-
Al-Fumarate	MOF	Commercial	-	-	-	-	-	-	-

[a] 20/80 = 20% Xe, 80% Kr gas; [b] 50/50 = 50% Xe, 50% Kr gas; [c] 10/90 = 10% Xe, 90% Kr gas; [d] 400 ppm Xe, 40 ppm Kr, balance air (O_2, CO_2, N_2); [d] 400 ppm Xe, 40 ppm Kr, 78.1% N_2, 20.9% O_2, 0.03% CO_2 and 0.9% Ar; [e] ISO = Single-component isotherms; [f] 350ppm Xe, 35 ppm Kr, 78% N2, 21% O_2, 0.03% CO_2, and 0.9% Ar; [g] 1000 ppm Xe, 78.1% N_2, 20.9% O_2, 0.03% CO_2 and 0.9% Ar; [h] 5% Xe, 5% Kr, 90%N_2 (by volume); [i] 400 ppm Xe, 40 ppm Kr, balance N_2; [j] 400 ppm Xe, 40 ppm Kr, 21% O_2, balance N_2; [k] measured in mmol g^{-1}; [l] simulated Grand Canonical Monte Carlo; *SSA* = specific surface area; POC = porous organic cage, OMS = open metal site, HUMM = Hybrid Ultra-Microporous Material, COP = covalent-organic polymers, PAF = porous-organic framework.